2015-05-01

Ligament Model Fidelity in Finite Element Analysis of the Human Lumbar Spine

Mitchell Scott Hortin
Brigham Young University - Provo

Ligament Model Fidelity in Finite Element Analysis of the Human Lumbar Spine

Mitchell Scott Hortin

A thesis submitted to the faculty of
Brigham Young University
in partial fulfillment of the requirements for the degree of

Master of Science

Anton E. Bowden, Chair
Stephen K. Charles
Eric R. Homer

Department of Mechanical Engineering

Brigham Young University

May 2015

ABSTRACT

Ligament Model Fidelity in Finite Element Analysis
of the Human Lumbar Spine

Mitchell Scott Hortin
Department of Mechanical Engineering, BYU
Master of Science

The purpose of this project is to quantify the effects of increasing spinal ligament fidelity on the mechanics of the human lumbar spine using finite element analysis (FEA). In support of this goal, a material characterization study was completed to provide anisotropic, nonlinear material parameters for the human anterior longitudinal ligament. (ALL).

Cadaveric samples of the human ALL were tested using a punch test technique. Multi-axial force-deformation data were gathered and fit to a commonly used transversely isotropic material model using an FEA system identification routine. The resulting material parameters produced a curve that correlated well with the experimental curve ($R^2 \geq 0.98$).

Recently published material data on several major spinal ligaments have been incorporated into an existing finite element model of the human lumbar spine. This data includes the results from the above mentioned material characterization, similar material characterizations of the supraspinous (SSL) and interspinous (ISL) ligaments, localized material properties of the SSL and pre-strain data for the ISL, SSL and ALL. These results have been incorporated both separately and compositely into the finite element model and each configuration has been simulated in spinal flexion, extension, axial rotation and lateral bending.

Results suggest that the effects of increased ligament model fidelity on bone strain energy were moderate and the effects on disc pressure were slight, and do not justify a change in modeling strategy for most clinical applications. There were significant effects on the ligament stresses of the ligaments that were directly modified, suggesting that these phenomenon should be included in FE models where ligament stresses are the desired metric.

Keywords: ligament, spine, finite element analysis, ALL, biomechanics

ACKNOWLEDGEMENTS

The body of work presented here would not be possible without the multitude of persons who helped make it possible. I would like the members of BABEL, particularly those who worked in the ligament characterization and FEA groups. I would like to thank my committee members Dr. Charles and Dr. Homer for their advice and guidance. I especially want to thank my advisor, Dr. Bowden, for helping me find projects that I am interested in and guiding me around and sometimes out of the pitfalls that I encountered along the way. Finally, I want to thank my family and especially my wife Sarah for showing genuine interest in my research, supporting me when things weren't going well, and celebrating with me when they did. I also appreciate the funding received from the National Science Foundation (Grant No. 0952758).

TABLE OF CONTENTS

LIST OF TABLES vii

LIST OF FIGURES viii

1 Introduction 1

1.1 Problem statement 1

1.2 Summary 2

2 A review of material characterization and the finite element methods of modelling the mechanical properties of ligaments 3

2.1 Motivation 3

2.2 Role of ligaments in the body 4

2.3 Mechanical properties of ligaments 4

2.3.1 Anisotropy 4

2.3.2 Viscoelasticity 5

2.3.3 Nonlinearity 6

2.3.4 Inhomogeneity and in situ strain 7

2.4 Ligament material testing 8

2.4.1 Testing methods 8

2.4.2 Ligament testing challenges 9

2.5 History of modeling efforts 10

2.5.1 One-dimensional models 10

2.5.2 Two-dimensional models 10

2.5.3 Three-dimensional models 11

2.6 Summary and future research directions 12

3 Transversely isotropic material characterization of the human anterior longitudinal ligament 13

3.1 Introduction 13

3.2 Materials and methods 15
3.2.1 Testing specimen preparation 15
3.2.2 Anisotropic quarter punch test 16
3.3 Test set-up 17
3.3.1 Test procedure 19
3.3.2 Constitutive model characterization 19
3.3.3 System identification procedure 21
3.4 Results 21
3.4.1 Observations 23
3.4.2 Average response parameters 23
3.4.3 Soft tissue displacement profile validation 25
3.5 Discussion 26
3.5.1 Comparison with previous ALL constitutive studies 26
3.5.2 Comparison to other spinal ligaments 28
3.5.3 Limitations 28
3.5.4 Significance 29
3.6 Acknowledgements 30
4 Quantitative comparison of ligament formulation and pre-strain in finite element analysis of the human lumbar spine 31
4.1 Introduction 31
4.2 Materials and methods 32
4.2.1 Finite element model 32
4.2.2 Modifications 34
4.2.3 Updated material models 34
4.2.4 Localized SSL material parameters 35
4.2.5 In situ strain 36

4.2.6 Post-processing 38
4.3 Results 39
4.4 Observations 42
4.5 Discussion 45
4.6 Acknowledgements 48
5 Summary and future work 49
5.1 Summary of contributions 49
5.2 Topics for future work 49
References 51
Appendix A. Ligament stress results 57
A.1 Anterior longitudinal ligament 57
A.2 Supraspinous ligament 59
A.3 Interspinous ligament 61
Appendix B. Nucleus pulposus pressure results 64
Appendix C. Bone strain energy results 67
Appendix D. Torque-rotaton curves 69
Appendix F. Loading files 72
F.1 Updated material model syntax 72
F.2 Localized SSL material properties syntax 73
F.3 In situ strain keyword syntax 74
F.4 Beam material model syntax 75
F.5 Loading files 76
F.6 Supercomputer input decks 77

LIST OF TABLES

Table 3-1: Nonlinear, anisotropic material parameters for the anterior longitudinal ligament....22

Table 4-1: Element types and material parameters for bone and discs....33

Table 4-2: Ligament material parameters for control model....33

Table 4-3: Updated material parameters....36

Table 4-4: Beam model ligament parameters....37

Table 4-5: Simulation case numbers....38

LIST OF FIGURES

Figure 2-1: Typical load elongation curve for a ligament showing the non-linear toe region, linear region and failure 7

Figure 3-1: Location of the anterior longitudinal ligament on the vertebrae 14

Figure 3-2: Finite element model of the AQPT experimental setup showing the initial state (left) and the deformed state (right). The green elements represent a rigid body that is displaced vertically. 17

Figure 3-3: Schematic showing the layout of the experimental apparatus showing 1) the profile cameras; 2) the mobile punch stage; 3) the location of the ligament sample; 4) the stationary stage 18

Figure 3-4: Close up of the AQPT testing stages showing 1) the mobile punch stage and 2) the stationary stage. The highlighted (green) areas represent the clamped segments of the ligament sample and the shaded (purple) represents the deformed quarter circle section of the ligament sample. 19

Figure 3-5: Typical correlation of force displacement data between experimental curve and the optimized solution 24

Figure 3-6: Solid line shows the average stress at each strain value. The average response values reported approximate these values. Error bars show the standard deviation at each point. Also shown is the stress strain curve produced by using the numerical average of each parameter. 24

Figure 3-7: Profile validation showing experimental profile (top), computer simulation profile (middle) and an overlay of the visible portions of the experimental profile on the computer profile (bottom) to emphasize similarities. 26

Figure 3-8: Average value and standard deviation comparison of fiber stiffness for the ALL according to different studies 27

Figure 4-1: Average nucleus pulposus pressure across all discs for each case and mode of bending 39

Figure 4-2: Average bone strain energy across all vertebrae for each case and mode of bending 40

Figure 4-3: Range of motion for each case and mode of bending 40

Figure 4-4: Average von Mises stress in the ALL for each case and mode of bending 40

Figure 4-5: Average von Mises stress in the SSL for each case and mode of bending 41

Figure 4-6: Average von Mises stress in the ISL for each case and mode of bending 41

Figure 4-7: Average von Mises stress in the PLL for each case and mode of bending 41

Figure 4-8: Average von Mises stress in the ligamentum flavum for each case and mode of bending 42

Figure 4-9: Average von Mises stress in the capsular ligaments for each case and mode of bending 42

Figure 4-10: Typical CPU hours required to complete a full simulation for each case 46

Figure A--1: Average ALL von Mises Stress in T12-L1 57

Figure A--2: Average ALL von Mises Stress in L1-L2 57

Figure A--3: Average ALL von Mises Stress in L2-L3 58

Figure A--4: Average ALL von Mises stress in L3-L4 58

Figure A--5: Average ALL von Mises stress in L4-L5 58

Figure A--6: Average ALL von Mises stress in L5-S1 59

Figure A--7: Average SSL von Mises stress in T12-L1 59

Figure A--8: Average SSL von Mises stress in L1-L2 59

Figure A--9: Average SSL von Mises stress in L2-L3 60

Figure A--10: Average SSL von Mises stress in L3-L4 60

Figure A--11: Average SSL von Mises stress in L4-L5 60

Figure A--12: Average SSL von Mises stress in L5-S1 61

Figure A--13: Average ISL von Mises stress in T12-L1 61

Figure A--14: Average ISL von Mises stress in L1-L2 61

Figure A--15: Average ISL von Mises stress in L2-L3 62

Figure A--16: Average ISL von Mises stress in L3-L4 62

Figure A--17: Average ISL von Mises stress in L4-L5 62

Figure A--18: Average ISL von Mises stress in L5-S1 63

Figure B--1: Average nucleus pulposus pressure in T12-L1 64
Figure B--2: Average nucleus pulposus pressure in L1-L2 64
Figure B--3: Average nucleus pulposus in L2-L3 65
Figure B--4: Average nucleus pulposus pressure in L3-L4 65
Figure B--5: Average nucleus pulposus pressure in L4-L5 65
Figure B--6: Average nucleus pulposus pressure in L5-S1 66
Figure C--1: Average strain energy in L1 67
Figure C--2: Average strain energy in L2 67
Figure C--3: Average strain energy in L3 68
Figure C--4: Average strain energy in L4 68
Figure C--5: Average strain energy in L5 68
Figure D--1: Angles of rotation during positive axial rotation 69
Figure D--2: Angles of rotation during negative axial rotation 69
Figure D--3: Angles of rotation during flexion.....70
Figure D--4: Angles of rotation during extension.....70
Figure D--5: Angles of rotation during positive lateral bending 70
Figure D--6: Angles of rotation during negative axial rotation 71

1 INTRODUCTION

1.1 Problem statement

Finite element analysis has become an essential tool in the study of biological systems such as the human lumbar spine. These analyses are essential to our understanding of the mechanics of the spine and give insight into the causes and possible treatment of conditions such as lower back pain and disc herniation. However, the complex nature of these systems and a lack of experimental data often lead to assumptions and simplifications which have the potential to produce inaccurate results.

In FE analysis of the spine, a major area of simplification is the representation of the spinal ligaments. Due to the lack of experimental data, they are often modeled as one-dimensional line elements, which act as linear springs. This method does not account for the three-dimensional anisotropic nature of ligaments and has the potential to produce misleading results. The purpose of this research twofold: to investigate the complex nature of ligaments with the goal of providing anisotropic material parameters for the human anterior longitudinal ligament that can easily be incorporated into a finite element simulation, and to use this data in conjunction with the results from similar studies to implement a more comprehensive model of the spinal ligaments in a previously validated FE model of the human lumbar spine. We anticipate that the results of this comprehensive model, when compared to results from a simplified model, will give insight into the role the complex nature of ligaments plays in the mechanics of the spine.

1.2 Summary

Chapter 2 constitutes a literature review focused on the finite element modeling of ligaments and ligament material characterization. One-dimensional, two-dimensional, and three-dimensional models are explained and compared with respect to accuracy and complexity. Future research directions in this area are also discussed.

Chapter 3 includes a peer-reviewed article on the characterization of the human anterior longitudinal ligament (ALL) that has been published in Journal of the Mechanical Behavior of Biomedical Materials. The methods section describes the details of the experimental procedure. The results section reports anisotropic material parameters for the ALL that can easily be incorporated into a finite element model. The discussion section compares the results with previously reported data from the literature.

Chapter 4 includes an article detailing the effects of increasing ligament model fidelity on the mechanics of the spine. The methods sections explains how ligament model fidelity was increased. The results section quantifies the results by comparing intervertebral disc pressure, ligament stresses, bone strain energy and torque – rotation curves. The discussion section explains the implications of the results as they apply to spine mechanics.

Chapter 5 provides a summary of the thesis and suggests future research directions.

2 A REVIEW OF MATERIAL CHARACTERIZATION AND THE FINITE ELEMENT METHODS OF MODELLING THE MECHANICAL PROPERTIES OF LIGAMENTS

2.1 Motivation

The complexity of biological systems makes them difficult to analyze using traditional mathematical methods, and the finite element method has become the tool of choice. The accuracy of these finite element models is driven by the accuracy of the parameters that are input into the system, the way the materials are represented and the assumptions that are made. This work focuses on the efforts to produce constitutive parameters for ligament tissue and accurately model the ligament components of a biomechanical system. Ligaments provide stability and passive resistance to motion, and therefore have a large effect on the overall response of the entire system[1]. As the accuracy of the ligament models increases, so does the accuracy of the entire system model and as the accuracy of a system model increases, so does the understanding of how that system works. The data that comes from accurate biomechanical models can improve our ability to understand and treat injuries and degenerative diseases.

An advantage of FEA modeling is that accurate experimental testing of ligaments is difficult. In vivo testing is not possible without causing permanent damage to the subject and experiments on dissected tissue has challenges in keeping the tissue alive and gripping the soft tissue[2]. Finite element testing allows for a testing environment that is repeatable, easily manipulated and has a relatively low cost.

2.2 Role of ligaments in the body

Ligaments provide stabilization to many of the joints in the body and restrict abnormal joint motion. In some joints, such as the shoulder, the ligaments are generally lax when the joint is in a neutral posture. When the shoulder reaches the extremes of its range of motion, the ligaments are put in tension and rapidly restrict further motion. Other joints, such as the knee, contain ligaments that are under tension even in neutral position. This tension, referred to as the in situ stress, is responsible for much of the joint stability [1].

The ligaments, along with muscle forces and inertial properties of bone, are responsible for the joint kinematics in each joint. It is therefore necessary to understand and accurately represent ligament forces in the system of interest in order to predict system response to a given input.

2.3 Mechanical properties of ligaments

This section will focus on the mechanical properties of ligaments that can cause difficulty or complexity in modeling. Included will be a brief review of the efforts to represent each mechanical property in the literature.

2.3.1 Anisotropy

One of the defining properties of ligaments is their anisotropic stiffness, which is due to the structural makeup of the ligament tissue. Ligaments are a composite material made up of a ground substance matrix and collagen fibers. This ground substance is primary composed of proteoglycans, glycolipids, fibroblasts and water. Water composes between 65 to 70% of the wet weight of most ligaments, and 70-80% of the remaining dry weight is made up by the collagen fibers[1]. These fibers are aligned parallel to each other in the direction of the primary stress in the ligament and are much stiffer than the matrix material. As a result, ligaments are much stiffer in

the direction along these fibers than in the direction perpendicular to the fibers, when the tensile force acts primarily on the ground substance.

Efforts at representing this behavior have been made since the earliest FE models. The simplest models represent ligaments as discrete line elements. [3-11] This is by far the most common method as it reduces model complexity while still retaining much of the ligament kinematics. Anisotropy is enforced by placing the line element parallel to the line of action of the ligament. Two-dimensional elements have been used to capture the data that one-dimensional models could not, such as inter-ligament stresses. Anisotropy has been introduced into these two-dimensional models by creating a composite of the previously mentioned line elements to represent the fibers and isotropic, linear elastic quadrilateral elements to represent the matrix[2]. Three-dimensional elements are used in more detailed models and more completely capture the three-dimensional behavior of ligament. Anisotropy is included in 3D elements by creating a composite of line elements in a matrix of 3D elements [12, 13], such as 8-noded hex elements, or by creating a continuum model with transversely isotropic material parameters [14-16].

2.3.2 Viscoelasticity

Ligaments have been shown to have viscoelastic properties, meaning they exhibit hysteresis under cyclic loading, stress relaxation and creep [1], however there is some controversy over the severity of the effect of this viscoelastic behavior [2]. Viscoelasticity is caused by the interactions between the collagen fibers, the ground substance and water. This viscoelastic behavior causes a hysteresis in the stress strain curve, signifying that energy is lost in the act of stretching the ligament. Ligaments also exhibit a history-dependent behavior, such that under repeated loading, the ligament becomes less stiff.

Efforts to include viscoelastic behavior into finite element representations of ligaments have focused on implementing viscoelastic material models in the elements used [17-19]. In one study, Sadegh et al [17] carried out dynamic loading simulations on an FE model of the cervical spine with and without viscoelastic material properties. They found that the viscoelastic model showed a maximum vertebral stress that was 22% less than that of the elastic model. They believed that this decrease was due to the fact that the impulse load was absorbed by the viscoelastic properties of the intervertebral discs and ligaments.

2.3.3 Nonlinearity

Experimental data has shown the load-elongation curve for ligaments to have a nonlinear section at low levels of strain, and then a linear region until failure (see figure 2-1). It is thought that the initial nonlinear section is due to the fact that in a zero strain position, the collagen fibers are in a crimped configuration, and at a low strain the fibers are in the act of straightening, resulting in a nonlinear load-elongation curve until the fibers are completely straightened, at which point the load-elongation curve becomes linear.[2] This behavior has been modeled by defining non-linear spring constants for the discrete line elements [6, 7, 9, 20-22], or by implementing a constitutive model that mimics this behavior.[12, 13, 16, 23]

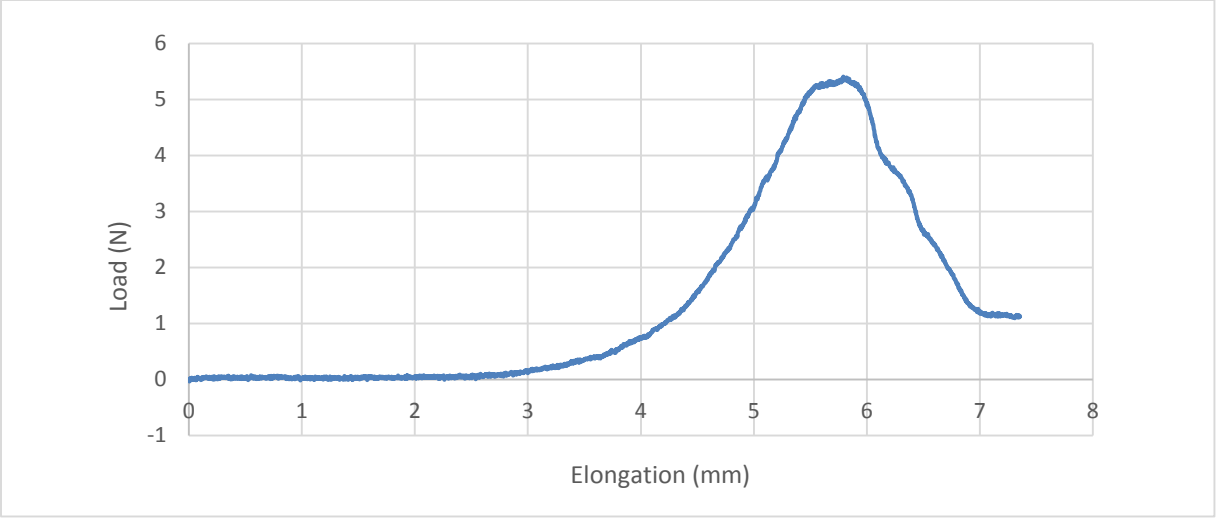

Figure 2-1: Typical load elongation curve for a ligament showing the non-linear toe region, linear region and failure

2.3.4 Inhomogeneity and in situ strain

It is commonly assumed in finite element models that the ligaments have the same material properties throughout the ligament geometry. A recent study done on the supraspinous ligament in the spine has shown that it exhibits a higher stiffness in the ventral region when compared with the dorsal region.[23] A similar study on ligaments of the knee found that the stiffness varied depending on the distance from the insertion sites.[24] It can be safely assumed that most ligaments will have variable material properties at different positions in their geometry. There are some system level finite element models that implement different amount of 1D line elements to approximate ligament inhomogeneity [25, 26] but this is harder to implement in more detailed models that use 3D representations, and is generally neglected.

Additionally, it is widely assumed in finite element models of ligaments that they are in a relaxed state at a neutral position in vivo. A recent study on the major ligaments of the spine has shown that the ligaments exhibit a varying amount of strain when the spine is in a neutral

posture.[15] Other studies have found that ligament in situ strain can have a significant impact on joint kinematics[27] and can contribute to joint stability when there is no active muscle force.[15] There is little ligament in situ strain data available in the literature so most models neglect in situ strain or assume a uniform in situ strain. There is at least one finite element model in the literature that implements experimental ligament in situ[28] but this the exception rather than the rule and it is focused on one ligament rather than a large system such as the spine.

2.4 Ligament material testing

Methods for gathering ligament material data can be designed or modified to measure specific aspects of ligament behavior. For example, traditional tension tests can be run cyclically to investigate the ligament response to cyclic loading[29]. Stretch and hold methods have been used to investigate creep and stress relaxation properties [30, 31]. This section will focus on tension testing techniques used to gather load-deformation data.

2.4.1 Testing methods

The simplest and most common tension testing technique is uniaxial tensile testing [32-34]. These tests provide data along one axis, traditionally in the direction of the ligament fibers. Data for a different axis requires a separate test and sample, which can introduce error into the study due to inter-specimen variability.

Consequently, planar biaxial testing has been developed in an attempt to gather multi-axial material data from a single sample [35, 36]. This method utilizes a square planar sample that is pulled along each edge, allowing collection of multiaxial data. The boundary effects of this method limit the viable test region to a small central portion of the tissue [37] and thus require relatively large sample sizes (3 to 6 cm square)[35]. Additionally, biaxial testing requires two inputs

(longitudinal and transverse forces) and the results are dependent on the combination of these two inputs.

Another method of multi-axial testing is a punch test technique which uses a circular punch to displace the ligament tissue. The method has been used to gather multi axial deformation data from relatively small sample sizes(e.g., 10 mm square)[38]. Additionally, a punch test captures an important mode of in vivo loading that is not obtained from uniaxial and biaxial planar testing techniques. An alternate version of this method that uses only a quarter circle segment of tissue has also been developed [23].

2.4.2 Ligament testing challenges

In addition to the aforementioned difficulties, the testing of ligament tissue can produce experimental challenges. The predominant challenge is gripping the ligament tissue in a way that does not interfere with the experimental process but can still produce tension in the ligament. Ligament samples are prone to slip from mechanical clamps during testing or to fail at the tissue-clamp interface due to stress concentrations in the compressed tissue. This has been avoided by using dry ice or liquid nitrogen to harden the tissue that is gripped by the clamps in order to avoid slippage or failure [39, 40]. Another method is to cut dog bone shaped segments out of the ligament tissue which ensure failure in the midsection of the tissue due to the decreased cross sectional area[32].

2.5 History of modeling efforts

2.5.1 One-dimensional models

The simplest method of modeling ligaments is to represent them as one-dimensional discrete line elements that act as tension only springs. This is the earliest and most common method of modelling ligaments[3-11] especially in system level models because it reduces the complex mechanics of the ligament to that of a spring yet still allows for the prediction of joint kinematics. The spring characteristics can vary in complexity from linear elastic[41] to nonlinear viscoelastic[17]. The force deflection relationship can be set to replicate the load elongation curve of a typical ligament. This is typically done by implementing a non-linear (typically quadratic) function at low strain levels and a linear function at higher strain levels[9]. The number of line elements used to represent one ligament can vary from one in the simplest case, to several in an attempt to model ligament inhomogeneity.[25, 26] The disadvantages of this approach are that it cannot predict stresses in the ligament tissue and that load cannot be transferred between the ligaments and surrounding tissue at any point other than the insertion point. In the body, the ligaments often wrap around each other or around bones, causing load transfer at many points along the length of the ligament[2].This behavior is not captured in a one-dimensional representation of ligaments.

2.5.2 Two-dimensional models

Two-dimensional representations of ligaments can capture more of the material response, such as inter-ligament stresses, but are still computationally simple when compared with three-dimensional elements. Results from two-dimensional models [42, 43] have shown that there are

regions of ligament tissue that are subject to shear and compressive loading, a behavior which one-dimensional representations are not able to predict.

2.5.3 Three-dimensional models

Three-dimensional models are the most fidelic and come closest to capturing the true material response of ligament. This method is rarely used, however, due to its complexity and the computational expense. Three-dimensional representations are more common in detailed analyses of one or few ligaments[12, 13, 23, 44, 45], and less common in system level models[46]. Three-dimensional representations can take the form of three-dimensional networks of discrete elements[47] or continuum models that use constitutive material models of varying complexity.[2, 16] Discrete element networks are essentially line elements connected in series by a linear spring and in parallel by dashpots. These are attractive because they use simple line elements and can capture a 3D response, but it can be difficult to assign material parameters to each individual element. Continuum models are more common. Some use isotropic material models which can predict experimentally determined behaviors [44], but have inherent errors due to their inability to represent the anisotropic structure of ligaments. Transversely isotropic constitutive models have been developed[48] that describe an isotropic matrix with reinforcing fibers. These material models can be used to model anisotropy in three-dimensional continuum models.

One common problem when modeling ligaments with volumetric elements is that they are very thin, and would require an inordinate amount of elements to maintain good aspect ratios. Shell elements can be used as an alternative in such a situation.[16] Shell elements have been formulated for bending of thin structures and are easier to mesh than solid elements[49]. Shell elements have been used when implementing a three-dimensional ligament representation in system level models [15, 46, 50].

2.6 Summary and future research directions

In summary, there are different methods that have been used to model the mechanical properties of ligaments with varying degrees of fidelity. The complexity of the ligament model is often determined by the size of the overall finite element model and the property being investigated. 3D continuum elements with a transversely isotropic material model provide the most true to life results, but the complexity of the system in question may make this representation unreasonable in many situations and 1D line elements may be the most appropriate. Shell elements can be used as a compromise for thin ligament sections.

There is much experimental research to be done in quantifying ligament in situ strain and inhomogeneity. While it is known that ligaments are inhomogeneous and exhibit in situ strain, the lack of experimental data causes many investigators to either make assumptions or neglect these properties altogether. The inclusion of these properties could have a significant impact in the response of system-level finite element models.

3 TRANSVERSELY ISOTROPIC MATERIAL CHARACTERIZATION OF THE HUMAN ANTERIOR LONGITUDINAL LIGAMENT

3.1 Introduction

Finite element analysis has become an important tool in understanding the biomechanical consequences of spinal degeneration, disease and treatment[51]. The accuracy of a finite element analysis relies heavily on the material models and parameters used to represent the spinal components, such as ligaments and bones. Therefore, it is important to utilize accurate and comprehensive material parameters for spinal ligaments to ensure model accuracy and utility [16]. This study focuses on the anterior longitudinal ligament, which runs along the anterior side of the entire vertebral column (see Figure 3-1). Transection of this ligament has been shown to cause an increased loading in the adjacent vertebral bodies [52] which could lead to bone or disc degeneration [53] if damaged or removed. All ligaments are known to exhibit non-linear, anisotropic properties [54] and while the response of other spinal ligaments has recently been reported [23, 55], the nonlinear anisotropic constitutive response of the ALL has not yet been defined in a way that allows it to be easily implemented in an FEA setting.

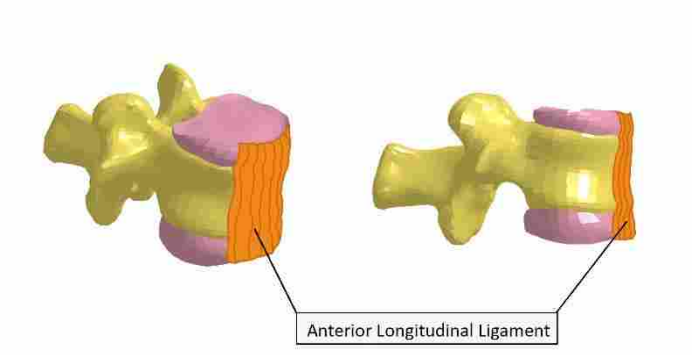

Figure 3-1: Location of the anterior longitudinal ligament on the vertebrae

Previous work on characterizing the ALL has relied on uniaxial testing [56, 57] and has primarily reported data on the ligament tensile strength and Young's modulus (i.e., linear ligament stiffness) of the ligament. These quantities are useful when modeling the ligament as a linear elastic spring, which is common in many finite element models [6, 10, 11]. However, finite element modeling of other joints has demonstrated a significant increase in accuracy with more fidelic constitutive material models to represent the anisotropic, nonlinear properties of the ligament. This is particularly the case when the ligament is the main focus of the model and a three-dimensional representation of ligaments is used [12, 23]. For these more fidelic models, additional constitutive parameters are necessary to completely define the material response of the ligament. Inclusion of nonlinear, anisotropic properties for spinal ligaments could similarly improve the fidelity of finite element models of the spine. However, to date, limited anisotropic material characterization data is available for spinal ligaments.

One of the impediments to acquiring anisotropic material constitutive parameters for spinal ligaments has been that traditional material testing techniques commonly require an entire functional spinal unit (ligament with 2 attached vertebrae) [34, 56]. Additionally, independent samples are required in order to obtain off-axis properties of the ligament. Thus, priority is given to characterizing the dominant (fiber direction) properties. Recent work has been done in planar

biaxial testing [36, 58], which represents a significant step forward in characterizing the anisotropy of soft tissues. Planar biaxial testing utilizes a square planar sample that is pulled along each edge of the sample, allowing collection of anisotropic data from a single sample. The boundary effects of this method limit the viable test region to a small central portion of the tissue[37] and thus require relatively large sample sizes (3 to 6 cm square)[58]. Additionally, biaxial testing requires two inputs (longitudinal and transverse forces) and the results are dependent on the combination of these two inputs. In recent work, the Anisotropic Small Punch Test (ASPT) [23] has been demonstrated to accurately characterize the nonlinear, anisotropic constitutive response based on a single multi-axial test of a single, very small testing specimen (e.g., 10 mm square samples with a 0.5 mm thickness). Additionally, a punch test captures an important mode of in vivo loading that is not obtained from uniaxial and biaxial planar testing techniques. In the present work, an alternative version of the ASPT known as the anisotropic quarter punch test (AQPT) is utilized to characterize the material constitutive behavior of the ALL. The AQPT eliminates the potential for the central punch of the ASPT to pierce the ligament, as well as a potentially higher discrimination between the deformation profiles of the orthogonal directions of the testing as compared to the ASPT.

3.2 Materials and methods

3.2.1 Testing specimen preparation

Two cadaveric spines (29 year old female, 80 lbs, 61 inches tall, 42 year old female, 145 lbs, 63 inches tall) were obtained from an accredited tissue bank following an IRB approved acquisition and testing protocol. Anterior longitudinal ligament segments were then individually excised from thoraco-lumbar spinal sections, flash frozen, and stored in a -20° C freezer. Prior to

testing, the ligaments were thawed and allowed to reach room temperature and sectioned approximately 2 mm thick using a microtome blade. Testing specimens with dimensions of 10 x 10 mm were cut from the sectioned tissue. In total, 2 cadaveric spines yielded 30 viable testing specimens from 14 ALL ligament segments. Prior to testing, the exact thickness of each specimen was measured using calipers. During dissection, handling and testing, specimens were spritzed with an isotonic saline solution every 5-10 minutes to keep them hydrated. All testing was conducted at room temperature.

3.2.2 Anisotropic quarter punch test

The chosen test method is an advanced version of the anisotropic small punch test (ASPT) known as the anisotropic quarter punch test (AQPT). This method vertically displaces the inner portion of a quarter-circle shaped section of the testing sample using a motorized linear actuator while holding the outer portion fixed (see Figure 3-2). Thus tension is produced in every direction of the 90° arc of the quarter circle including a direction parallel to the ligament fibers and a direction perpendicular to the fibers. This multiaxial test allows collection of constitutive data from both the ligament fiber response and the ligament matrix response during testing of a single sample. Separation of the corresponding constitutive parameters is accomplished using a post-testing system identification procedure. For collagenous tissues with a primarily single-fiber direction, such as the ALL, the orientation and geometry of the testing samples also provide a directly observable validation response that can be optically measured during testing. Specifically, the edge of the quarter-circle shaped sample that is aligned with the fiber direction is pulled taut during testing, while the edge of the sample that is orthogonal to the fiber direction exhibits a noticeable "sag". Quantification of these displacement "profiles" of the sample edges provides an

independent and measurable validation of the accuracy of the constitutive parameters computed during the system identification procedure.

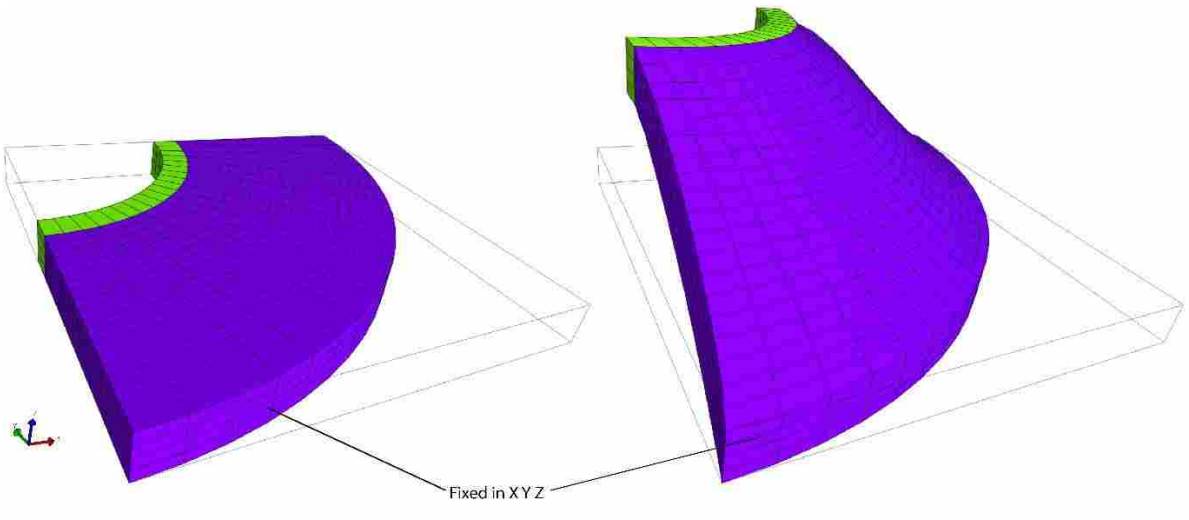

Figure 3-2: Finite element model of the AQPT experimental setup showing the initial state (left) and the deformed state (right). The green elements represent a rigid body that is displaced vertically.

3.3 Test set-up

CCD cameras (scA640-70fm, Basler Vision Technologies, Germany) equipped with macro zoom lenses (MLH-10X, Computar, New York) were mounted to capture pictures of the profiles of the ligaments during testing. One camera was mounted parallel to the fiber direction, while another was mounted perpendicular to the fiber direction (see Figure 3-3). These profile images can be compared to the FEA simulation profiles to provide a secondary validation of the results. A light source was mounted behind trace paper, one behind each camera view, acting as a diffuser to provide better contrast and therefore better images. The light source was only used intermittently (10 seconds at a time), and was mounted more than 6 inches from the specimens to ensure that the specimens did not experience measurable heating. Care was taken to ensure specimens did not dry out underneath the lamp by regularly spraying with saline solution.

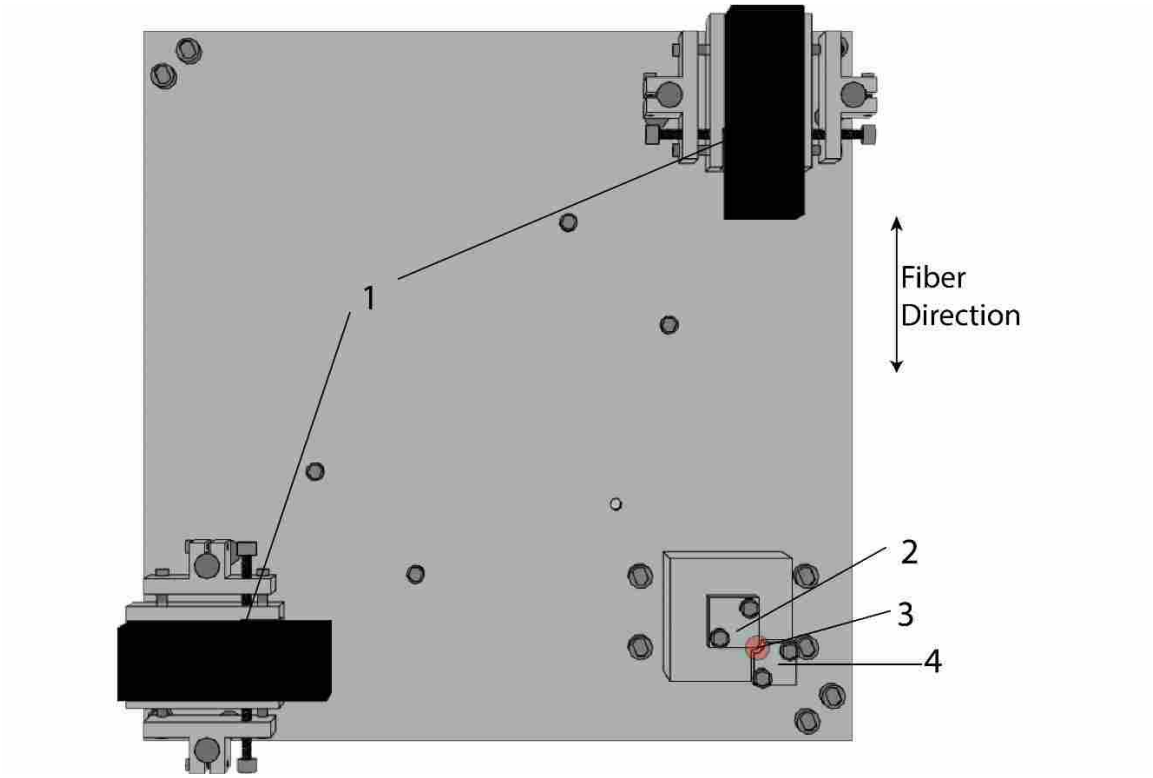

Figure 3-3: Schematic showing the layout of the experimental apparatus showing 1) the profile cameras; 2) the mobile punch stage; 3) the location of the ligament sample; 4) the stationary stage

Prior to testing, an electronic level was used to ensure that the stages began level, with no vertical gap between them. Specimens were loaded onto the test fixture with the fiber direction parallel to the left side of the immovable stage (see Figure 3-3). This ensured that the experimental model matched the FEA model for accurate data processing. Clamps were then placed over the specimens to keep them in place (see Figure 3-4). Velcro was attached to the bottom of the clamps and the top of the stages in order to avoid slipping of the specimen during testing. The specimen experiences a "quarter punch" during testing as the first stage has a quarter-circle shape that clamps a portion of the specimen, and as the stage rises, it punches the specimen, stretching it simultaneously both in the direction parallel to the ligament fibers and perpendicular to the fibers.

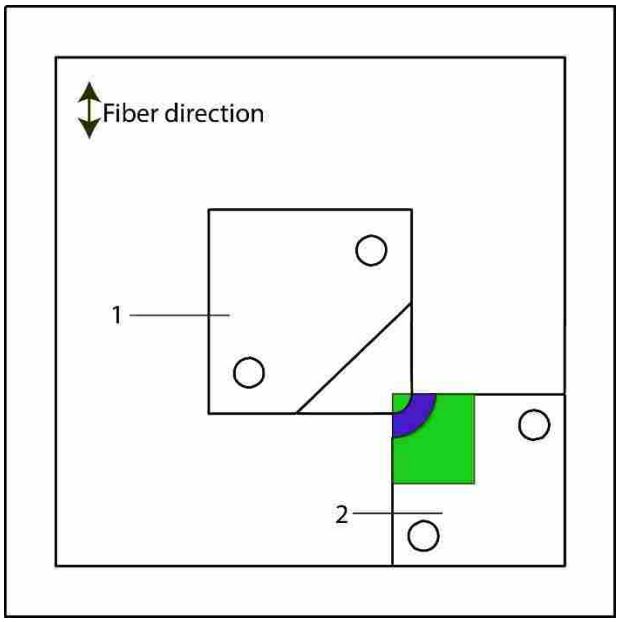

Figure 3-4: Close up of the AQPT testing stages showing 1) the mobile punch stage and 2) the stationary stage. The highlighted (green) areas represent the clamped segments of the ligament sample and the shaded (purple) represents the deformed quarter circle section of the ligament sample.

3.3.1 Test procedure

Stage 1 was displaced vertically at a rate of 0.125mm/s (see Figure 3-4). This was performed by a motor located underneath. The stage was elevated until failure of the ligament while both data and images were captured up until failure. Data was collected on the vertical displacement as well as force. The vertical displacement was measured with a LabView interface which recorded the movement of the motor. Force was measured by a load cell located between the motor and the stage. Sampling rate for the data was 100 Hz while the sampling rate for images was 10 Hz.

3.3.2 Constitutive model characterization

A finite element model simulation of the experimental test was developed so that it could be modified to mimic the experimental response of the ligament. The ligament material in the model is characterized using a strain-energy based continuum model developed by Weiss et al [48] which

expresses the strain energy in the ligament material as:

$$W = F_1(I_1) + F_2(\lambda) + F_3(I_1, I_2, \lambda) \quad (3\text{-}1)$$

Where W is the strain energy, F_1 describes the contribution of the matrix component to the strain energy, F_2 describes the contribution of the fiber components to the strain energy and F_3 describes the contribution of the interactions between the matrix and the fibers to the strain energy. F_3 is commonly assumed to be negligible compared to F_1 and F_2 and thus is neglected in this study. In our study, F_1 is described as Neo-Hookean material model where the strain energy is described in terms of constitutive parameters:

$$\frac{C_1}{2}(I_1 - 3) \quad (3\text{-}2)$$

where I_1 is the first invariant of the right Cauchy stretch tensor. This model assumes the matrix to be isotropic and incompressible and the way the fibers are organized gives a transversely isotropic response. The strain energy of the fibers can be written

$$\lambda W_\lambda = 0, \lambda < 1, \quad (3\text{-}3)$$

$$\lambda W_\lambda = C_3\left(e^{C_4(\lambda-1)} - 1\right), \lambda < \lambda^* \quad (3\text{-}4)$$

$$\lambda W_\lambda = C_5\lambda + C_6, \lambda \geq \lambda^* \quad (3\text{-}5)$$

where λ is stretch and W_λ denotes the first derivative of strain energy with respect to λ. The material model assumes that the toe region, the section of the stress strain curve that is nonlinear, is due to the uncrimping of the collagen fibers and can be represented by an exponential function. C_3 and C_4 represent the response during uncrimping of the fibers in the toe region. Finally, the model assumes that the linear region of the stress strain response is produced once the fibers are completely straightened and C_5 represents the modulus of the straightened fibers in the linear region. λ^* represents the stretch where the fibers switch from uncrimping to stretching (transition

from toe region to linear). C_6 is calculated as follows:

$$C_6 = C_3\left(e^{C_4(\lambda^*-1)} - 1\right) - C_5\lambda^* \quad (3\text{-}6)$$

3.3.3 System identification procedure

The experimental force displacement data is used to find material parameters that best imitate the experimental behavior of the ligament. This is done by running multiple simulations of the finite element model with different material parameters until the load displacement curve produced by the simulated model is sufficiently close to that of the experimental data. The optimization module in FEBio was used to implement this process as an automatically driven system identification process. FEBio uses a gradient based optimization routine to minimize the sum of the square of the difference (the residual) between the experimental data and the results of the computer simulation. The routine iterates until the difference reaches a minimum value, the change in parameters between iterations is minimal, or the program reaches a specified maximum number of iterations. Calculation of the final residual provides an objective measure of the systemic accuracy of the final constitutive parameters in representing the observed experimental behavior. Note that the system identification procedure does not utilize the edge profile data as part of its optimization procedure, thus this data provides an independent validation of the accuracy of the results.

3.4 Results

A total of 30 test specimens were prepared and tested to failure. Slippage was observed in nine of the test specimens, thus their results were discounted, and one set of data failed to converge in the optimization routine. A typical experimental load elongation curve along with the

corresponding optimized simulation results is shown in Figure 3-4. The optimized constitutive parameters for each valid test sample are reported in Table 1. The R^2 values reported quantify the degree of correlation between the experimental response and data generated by the constitutive model (see Figure 3-5). In each test, the R^2 value exceeded 0.98, indicating that the chosen constitutive model accurately simulates the ligament behavior.

Table 3-1: Nonlinear, anisotropic material parameters for the anterior longitudinal ligament

Level	*Sex*	*Age*	C_1*(MPa)*	C_3*(MPa)*	C_4	C_5*(MPa)*	Λ^*	R^2
T2-T3	F	29	0.103	0.760	4.099	12.044	1.088	0.9996
			0.026	0.020	2.580	6.070	1.253	0.9982
T9-T10	F	29	0.035	0.026	1.000	2.040	1.350	0.9982
			0.120	0.360	1.120	24.670	1.311	0.9987
T1-T2	F	42	0.104	0.317	1.000	23.327	1.168	0.9839
T2-T3	F	42	0.103	0.015	1.000	5.450	1.104	0.9931
T3-T4	F	42	0.084	0.609	4.430	14.230	1.120	0.9998
T4-T5	F	42	0.036	1.221	4.037	14.286	1.268	0.9996
T5-T6	F	42	0.100	1.310	5.096	11.220	1.215	0.9976
			0.088	0.061	10.063	22.180	1.354	0.9991
T6-T7	F	42	0.093	1.325	4.413	14.370	1.203	0.9989
			0.070	1.743	4.866	13.250	1.091	0.9967
			0.160	1.910	6.463	6.748	1.040	0.9992
			0.152	1.477	2.270	6.455	1.120	0.9983
T8-T9	F	42	0.094	1.490	4.135	14.670	1.094	0.9996
			0.012	1.033	4.437	16.161	1.371	0.9999
L3-L4	F	42	0.400	1.629	11.433	46.420	1.072	0.9962
			0.036	0.057	4.955	5.2817	1.144	0.9980
L5-S1	F	42	0.028	0.693	2.945	14.0544	1.377	0.9997
			0.058	0.091	1.205	5.600	1.680	0.9967
Numerical Average			**0.095**	**0.807**	**4.077**	**13.936**	**1.221**	**0.9976**
Std Dev			**0.081**	**0.648**	**2.744**	**9.707**	**0.150**	**0.004**
Average Response			**0.3**	**1.19**	**2.201**	**14.52**	**1.15**	**0.9892**

3.4.1 Observations

Each set of experimental data that was analyzed exhibited characteristics expected for ligament material (see Figure 3-5). At low levels of strain, the load elongation curves were non-linear, corresponding to the toe region where the ligament fibers are straightened from their original 'crimped' structure. At higher levels of strain, the load elongation curves became linear, corresponding to the region where the ligament fibers are fully straightened and carrying the majority of the ligament stresses. It is the slope of this region that is given to be the elastic modulus of the collagen fibers. In the chosen constitutive model, the C5 parameter represents the modulus of elasticity in the direction of the fibers when the fibers are fully uncrimped and is most easily compared with the modulus of elasticity reported from uniaxial tests. The values reported here for C5 are comparable with previously reported values for the modulus of elasticity of the ALL [34, 56].

3.4.2 Average response parameters

There is typically a large amount of variation in material responses of biological tissue, including ligaments [23, 55], and the present work is not an exception. Reported in Table 3.1 are the numerical averages for each of the constitutive parameters as well as the parameters that approximate the average stress response. These values were obtained by using the system identification procedure described above to find the material parameters that approximate the load elongation curve that produces the average stress strain curve (see figure 3.6). The average response parameters more accurately model the average material behavior and avoid errors associated with simple averages of experimental results [59].

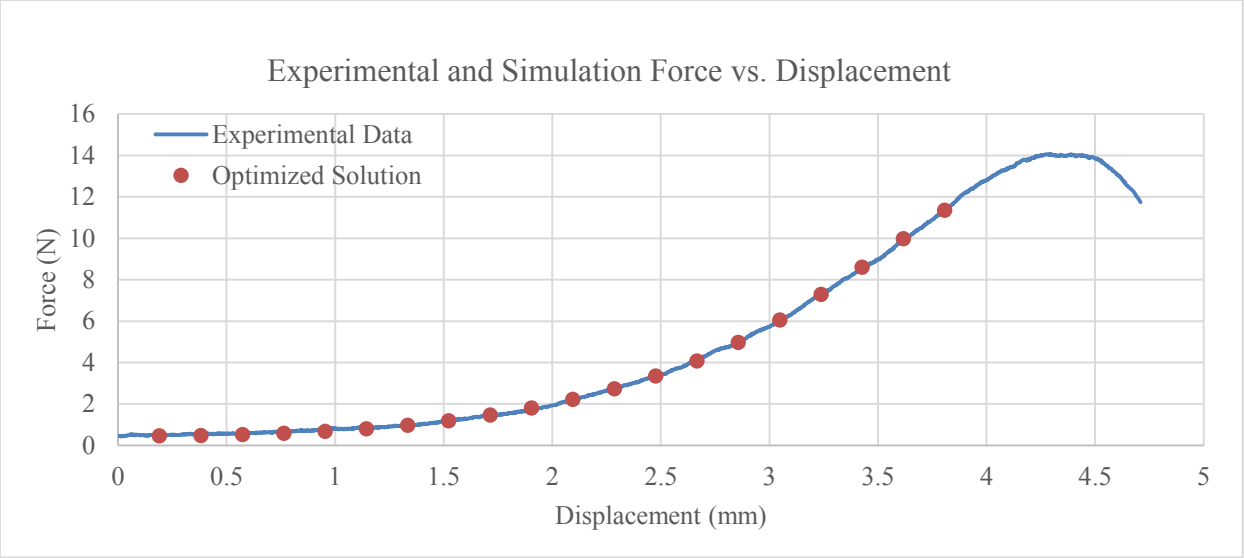

Figure 3-5: Typical correlation of force displacement data between experimental curve and the optimized solution.

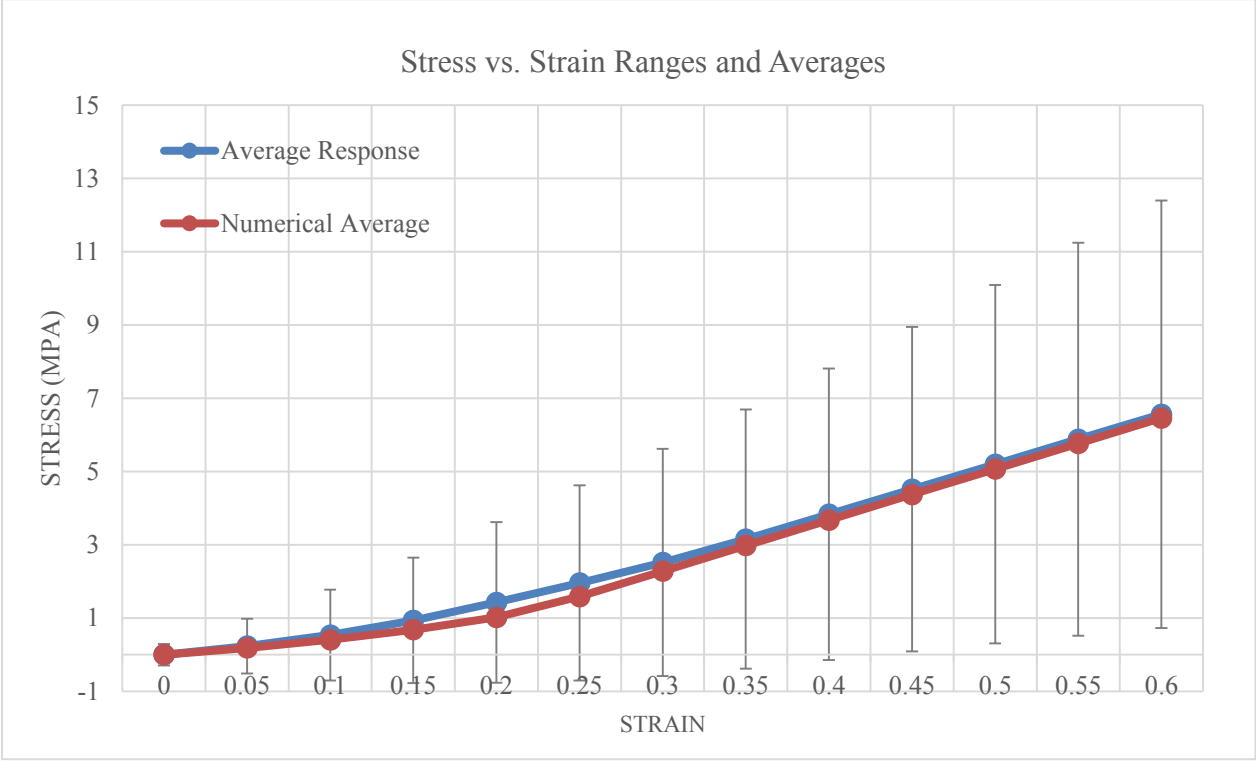

Figure 3-6: Solid line shows the average stress at each strain value. The average response values reported approximate these values. Error bars show the standard deviation at each point. Also shown is the stress strain curve produced by using the numerical average of each parameter.

3.4.3 Soft tissue displacement profile validation

The cameras mounted on the testing apparatus captured the profile of the ligament throughout the testing process. The profiles seen from these cameras show that in the fiber direction (which is aligned with one side of the testing specimen), the specimen displacement profile looks as though it was stretched taught, while the other side (perpendicular to the fiber direction) has a noticeable sag. This anisotropic displacement profile was expected and coincides with the mechanics of anisotropic tissue, and was accurately captured in the finite element simulation. Figure 3.7 shows the experimental profile next to the simulation profile as well as an overlay for comparison. It should be noted that the cameras were not perfectly perpendicular to the profile, which obscures part of the ligament profile. While the system identification process is rigorous enough to provide verified results, additional work quantifying the sensitivity of the displacement profile, as well as the potential for systematic error is needed before this methodology can be employed as a quantitative validation of the measured constitutive properties. For the present work, validation was obtained by 1) comparison with previously obtained fiber direction properties for the ALL (Section 3.4.1), and through comparison of the force-displacement response of experimental testing with the finite element analysis results. This method of validation is consistent with previously published work (e.g., Robertson et al [23]) supporting findings obtained through a similar system identification process.

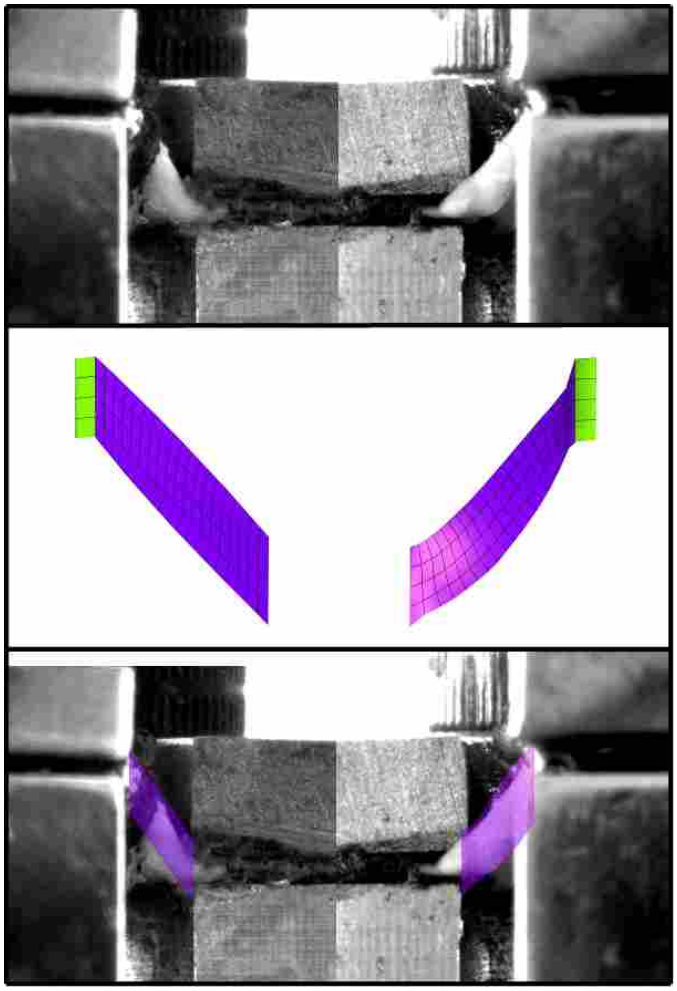

Figure 3-7: Profile validation showing experimental profile (top), computer simulation profile (middle) and an overlay of the visible portions of the experimental profile on the computer profile (bottom) to emphasize similarities.

3.5 Discussion

3.5.1 Comparison with previous ALL constitutive studies

Due to the fact that previous material characterization studies on the ALL reported isotropic parameters obtained from uniaxial testing in a single (fiber) direction, there cannot be a direct comparison of all parameters reported in this study. However, the C_5 parameter, which represents the elongated fiber stiffness along its major axis, can be compared to the stiffness values reported by these previous studies (see Figure 3-8) [34, 56]. On average, the fiber stiffness values reported

in this study are somewhat lower than those reported in previous studies, with the higher values in this study overlapping with the lower values reported in previous studies. This is most likely due to simple material differences between spinal samples (e.g., normal variability seen in working with biological tissues from distinct populations). It should be noted that the tighter range of reported fiber stiffness by Neumann et al. is most likely due to the fact that their study used samples almost exclusively from the lumbar spine, whereas the present study and Myklebust used samples from both the lumbar and thoracic spine. It is also a possibility the small size of the samples in the present work functions at a different level of the mechanical continuum (e.g., the density of collagen cross linkages may be different). Further studies investigating the influence of sample size and measured material properties may be required for further understanding as to whether this is a concern.

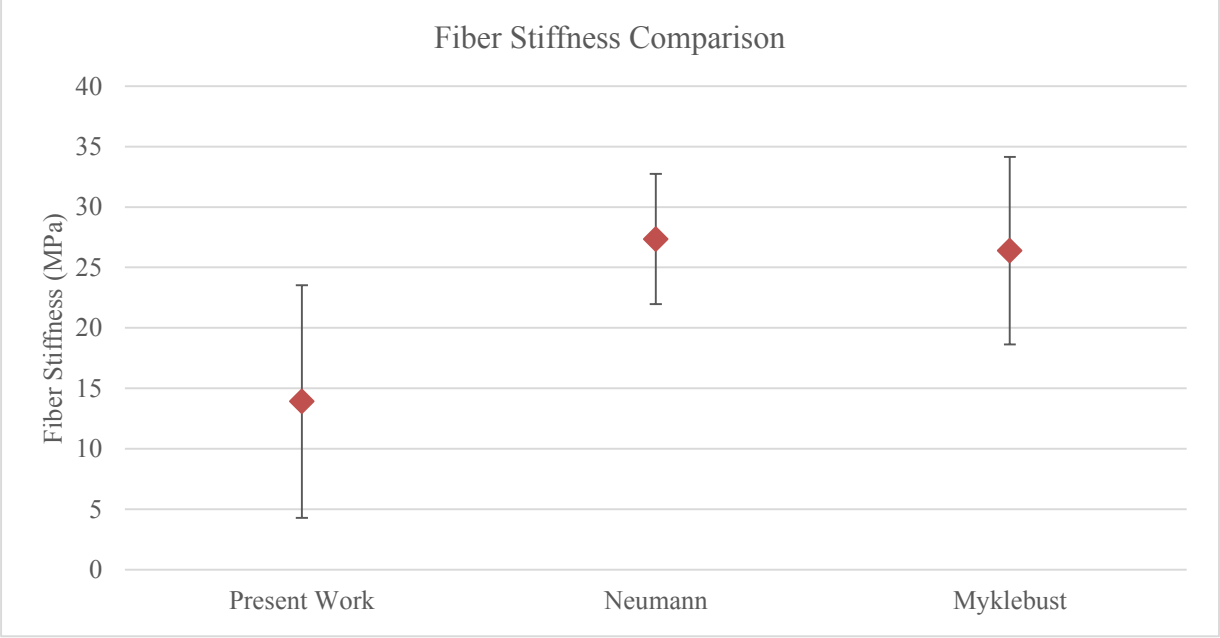

Figure 3-8: Average value and standard deviation comparison of fiber stiffness for the ALL according to different studies

3.5.2 Comparison to other spinal ligaments

Bradshaw[55] and Robertson[23] have previously conducted studies on the ISL and SSL respectively, using similar testing methods and the same material constitutive model as presented in this study. Their results suggest that both the ISL and the SSL have a higher average fiber stiffness, at 20.08 MPa and 19.24 MPa respectively, compared to 14 MPa for the ALL. Additionally, their studies indicate that both the ISL and SSL have a shorter nonlinear toe region, suggesting that the collagen fibers become completely straightened at lower levels of strain than that of the ALL. Their results show that the ISL and SSL fibers become straightened at 9% and 6% strain compared to 14% for the ALL.

Another point of comparison can be found in a study done by Chazal, et al. [60] who found that that the ALL has lower levels of stress at similar levels of strain (1.15 MPa at 12% strain) than the ISL and SSL(both reported as 1.75 MPa at 12% strain), indicating a lower stiffness. They also report results for the posterior longitudinal ligament (PLL)(2.04 MPa at 11% strain) and the ligamentum flavum (LF) (3.17 MPa at 6% strain). They report that the toe region for the ALL, SSL and ISL ends at 12% strain, for the PLL at 11% strain and for the LF at 6% strain. These results, though produced using different testing methods, similarly show that the ALL has a lower stiffness and longer toe region when compared with other major spinal ligaments.

3.5.3 Limitations

Post-testing comparison of the testing specimens that slipped during testing (and were thus excluded from the analysis) revealed that testing specimen geometry was likely the major source of difficulty. Specimens were cut using ad hoc scalpel techniques and the specimens with less orthogonal cut planes had a reduced specimen area between the grips and were more likely to slip. Future work would benefit from a custom-machined sample punch that would result in uniform

testing specimens. Additionally, there was one sample that represented a significant outlier with respect to the measured material response (almost double the average C_5 values of the other specimens). This outlier could be due to sample condition (e.g., desiccation) or perhaps inhomogeneity in the ligament itself.

A limitation of the present work is that the reported material parameters do not take into account the viscoelastic properties of the ALL. The elastic properties of the ALL dominate the physical response and the present work's inclusion of the nonlinear and anisotropic components of that response represents a significant step forward in available constitutive data for this important spinal ligament. However, all ligaments exhibit both rate-dependence and viscoelastic characteristics. Further studies in these areas are needed in order to fully characterize the behavior of this ligament.

3.5.4 Significance

We believe this is the first study to present transversely isotropic constitutive response for the human ALL. We have reported these parameters using a validated and commonly used material model for soft tissue that is already implemented in widely used Biomechanics FEA programs such as LS-DYNA and FEBio. Utilization of this constitutive model allows for straightforward application of our tested properties to already existing finite element models of the spine. The range of stress – strain values that result when implementing the reported material parameters are given in Figure 6. The high R^2 values indicate that these transversely isotropic material parameters can be used in conjunction with the Weiss model to accurately model the anisotropic material response of the human anterior longitudinal ligament. From a clinical perspective, there are several surgical procedures that routinely transect the ALL, notably anterior fusion devices and total disc replacement [61, 62]. Our current understanding of the consequences

of these transections has been limited due to a lack of anisotropic constitutive parameters. It is anticipated that the present work can be used to improve both our modeling and our understanding of the clinical consequences of these procedures.

3.6 Acknowledgements

I want to thank my coauthors Sarah Graham, Kara Griffiths, Peter Hyoung and Dr. Anton Bowden for their contributions to the methods, testing, analysis, and writing of this study.

4 QUANTITATIVE COMPARISON OF LIGAMENT FORMULATION AND PRE-STRAIN IN FINITE ELEMENT ANALYSIS OF THE HUMAN LUMBAR SPINE

4.1 Introduction

Finite element analysis of the spine has become a nearly indispensable tool that can enable direct comparisons of the biomechanical differences between possible treatments of disorders and injuries such as chronic lower back pain and disc herniation. Additionally, FE analysis enables investigators to avoid the challenges inherent in physical testing and provides a repeatable setting with precise control over material properties and boundary conditions.

This control also enables a wide variety in the fidelity of finite element analyses of the lumbar spine. Material models and boundary conditions are often simplified because of the high computational expense of complex analyses or because of a lack of experimental data, though it has been shown that higher fidelity models correlate better with physical testing. For example, inclusion of heterogeneous material properties in the cancellous bone of the vertebrae produced significant changes in bone strain energy when compared to results from a homogenous model.[63] Additionally, the major ligaments of the spine are often represented as uniaxial elastic springs [3, 64, 65] when in reality they exhibit a nonlinear, anisotropic behavior.[16] A study on ligament representation in the knee found a significant increase in correlation with physical testing while using a 3D anisotropic hyperplastic model compared to a uniaxial material model. [66] Differences in ligament results have also been seen with the inclusion of prestrains [27, 67] and inhomogeneous material properties [26] for the major knee ligaments. It can be assumed that these trend extends

to spinal ligaments. The effect of the inclusion of these phenomena into an FE model of the spine remains unclear as does the relative worth of increased fidelity compared to the increased computational cost.

Material parameters that detail the anisotropic, nonlinear response of the supraspinous (SSL)[23], anterior longitudinal (ALL)[68], and interspinous (ISL)[55] ligaments have recently been published. Additionally, Robertson et al[15] have published data quantifying the in situ strain of these three spinal ligaments and the geometrically localized properties of the SSL. In the current study, these results have been sequentially incorporated into a previously validated finite element model of the lumbar spine[52] to create a series of models with increasing fidelity of spinal ligament constitutive behavior. The results from these models are compared to each other and to a control model to gain insight into the role these ligament phenomena play in the mechanics of the lumbar spine and to identify whether the increased computational burden associated with including these advanced material constitutive characteristics is justified.

4.2 Materials and methods

4.2.1 Finite element model

The control model for this process is a finite element model previously developed and validated by Von Forell et al[52]. The model geometry is based on quantitative computed tomography (QCT) data from the cadaveric spine of a 65 year old female. The outer cortical bone was modeled using isotropic elastic shell elements, and the internal cancellous bone was modeled using density dependent hex elements. The density data for the cancellous bone was gathered from calibrated QCT data and then assigned to the corresponding computational element. The intervertebral discs

were modeled as three separate parts: the outer annulus fibrosis, inner annulus fibrosis, and the nucleus pulposus. (See Table 4-1)

Table 4-1: Element types and material parameters for bone and discs

Component	Element type and material model	Modulus(MPa)	Poisson's ratio	References
Cortical Bone	Isotropic elastic shell elements	12000	0.2	[31, 32]
Cancellous Bone	Density dependent orthotropic elastic hex elements	$E_z=4730\rho^{1.56}$ $E_x=0.42E_z$ $E_y=0.29E_z$	0.38 0.23 0.4	[35, 36]
Nucleus pulposus	Elastic fluid hex elements	1667.67	Incompressible	[37, 69]
Inner annulus fibrosis	Orthotropic elastic hex elements	5.59, 0.34, 0.19	1.77, 0.33, 0.14	[29]
Outer annulus fibrosis	Orthotropic elastic hex elements	20.9, 0.42, 0.29	2.27, 0.79, 0.61	[68]

The spinal ligaments included in this model are the anterior longitudinal ligament (ALL), posterior longitudinal ligament (PLL), ligamentum flavum (LF), supraspinous ligament (SSL), interspinous ligament (ISL), and the capsular ligaments at the facet joints. These ligament are modeled with shell elements using a nonlinear, tension only, fabric material model[38]. Cross sectional thickness values for each ligament are taken from reported values in the literature[60]. The nonlinear stress strain behavior of these ligaments was implemented as piecewise linear functions based on reported experimental data[60] (see Table 4-2).

Table 4-2: Ligament material parameters for control model

Ligament	Cross Sectional Area (mm^2)	Stress Strain Control Points		
		A	B	C
Anterior Longitudinal	65.6	0.12 ,1.15	0.44, 9.11	0.57 ,10.3
Supraspinous	15.1	0.17, 0.95	0.38, 5.86	0.54, 6.69
Interspinous	15.1	0.17, 0.95	0.38, 5.86	0.54, 6.69
Posterior Longitudinal	25.7	0.11, 2.04	0.34, 16.2	0.44 ,20.8
Ligamentum Flavum	39.0	0.07, 2.04	0.19, 9.14	0.25, 10.4

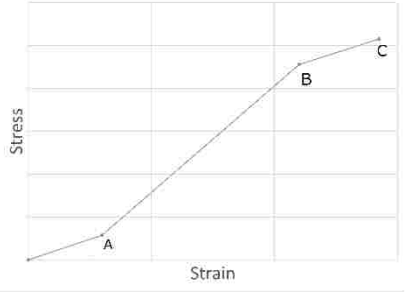

4.2.2 Modifications

Several modifications were made to the existing control model to incorporate recently published data on ligament behavior and for points of comparison.

4.2.3 Updated material models

Recent data has been published that quantifies the nonlinear, anisotropic material behavior of several major spinal ligaments. This data is formulated as six independent material parameters that describe ligament behavior using a transversely isotropic material model developed by Weiss et al [48] which expresses the strain energy in the ligament material as:

$$W = F_1(I_1) + F_2(\lambda) + F_3(I_1, I_2, \lambda) \quad (4\text{-}1)$$

Where W is the strain energy, F_1 describes the contribution of the matrix component to the strain energy, F_2 describes the contribution of the fiber components to the strain energy and F_3 describes the contribution of the interactions between the matrix and the fibers to the strain energy. F_3 is commonly assumed to be negligible compared to F_1 and F_2 and thus is neglected in this study. In this study, F_1 implemented as a Neo-Hookean material model where the strain energy is described in terms of constitutive parameters:

$$\frac{C_1}{2}(I_1 - 3) \quad (4\text{-}2)$$

where I_1 is the first invariant of the right Cauchy stretch tensor. This model assumes the matrix to be isotropic and incompressible and the way the fibers are organized gives a transversely isotropic response. The strain energy of the fibers can be written

$$\lambda W_\lambda = 0, \lambda < 1, \quad (4\text{-}3)$$

$$\lambda W_\lambda = C_3\left(e^{C_4(\lambda-1)} - 1\right), \lambda < \lambda^* \quad (4\text{-}4)$$

$$\lambda W_\lambda = C_5\lambda + C_6, \lambda \geq \lambda^* \quad (4\text{-}5)$$

where λ is stretch and W_λ denotes the first derivative of strain energy with respect to λ. The material model assumes that the toe region, the section of the stress strain curve that is nonlinear, is due to the uncrimping of the collagen fibers and can be represented by an exponential function. C_3 and C_4 represent the response during uncrimping of the fibers in the toe region. Finally, the model assumes that the linear region of the stress strain response is produced once the fibers are completely straightened and C_5 represents the modulus of the straightened fibers in the linear region. λ^* represents the stretch where the fibers switch from uncrimping to stretching (transition from toe region to linear). C_6 is calculated as follows:

$$C_6 = C_3\left(e^{C_4(\lambda^*-1)} - 1\right) - C_5\lambda^* \quad (4\text{-}6)$$

Experimental force deformation data was recorded for the SSL[23], ISL[55], and ALL[68] using a punch test technique. This data was compared with data from an FEA simulation of the physical experiment. This process was repeated in an optimization loop until the material parameters produced a force displacement curve that sufficiently matched that of the physical experiment.

These material parameters (see Table 4-3) were implemented into the finite element model by replacing the existing fabric material model for the SSL, ISL and ALL with a soft tissue material model implements the transversely isotropic material description as described above.

4.2.4 Localized SSL material parameters

In their study of the SSL [23], Robertson et al sectioned the ligament into dorsal, mid, and ventral sections. Each section was individually tested and parameters were published that show the differences in material properties for each section (see Table 4-3). To represent this behavior, the existing SSL geometry was duplicated twice to create three separate bodies, each assigned a thickness one-third that of the original body. The reference surfaces for the shell elements

representing the dorsal and ventral sections were adjusted an appropriate distance and the corresponding material parameters were applied.

4.2.5 In situ strain

Though the use of optical markers, Robertson et al has shown that the SSL, ALL, and PLL experience strain when the spine is in a neutral position[15]. This effect was quantified by comparing the relative location of optical markers *in situ* with their position when the ligament was excised from the spine and allowed to reach a strain free configuration (see Table 4-3). This was implemented by stretching isolated sections of the simulated ligaments to the appropriate strain in order produce history state variables for each section of the ligaments. These history variables were then used to implement an initial stress state for each ligament that corresponded to the correct initial strain. For the negative in situ strain in the SSL, the geometry of the SSL between each vertebrae was lengthened the appropriate amount to simulate negative strain.

Table 4-3: Updated material parameters

Soft tissue material models						
Ligament	Element Type and Material Model	Material Parameters				
		C_1	C_3	C_4	C_5	λ*
Anterior Longitudinal	Transversely isotropic soft tissue material shell elements	0.3	1.19	2.201	14.52	1.15
Interspinous		0.27	0.62	13.27	20.08	1.09
Supraspinous		0.17	0.6	11.88	19.24	1.06
In Situ Values						
Ligament	Location	Direction			% Strain	
Anterior Longitudinal	Bone	Transverse			4.5	
		Longitudinal			2	
	Disc	Transverse			1	
		Longitudinal			5.3	
Interspinous		Horizontal			3.7	
		Vertical			4.3	
Supraspinous		Longitudinal			-6.0	

Table 4-3 Continued

Localized SSL Material Parameters						
Ligament	Section	Material Parameters				
		C_1	C_3	C_4	C_5	λ*
Supraspinous	Dorsal	0.2	0.54	9.46	14.93	1.06
	Midsection	0.16	0.76	9.66	12.57	1.06
	Ventral	0.15	0.6	16.37	25.74	1.06

In addition to the modifications intended to make the model more fidelic, a model was also developed that used beam elements and a tension only cable material model for the ALL, SSL and ISL. This method is consistent with that implemented in other FE simulations of the spine [5, 7, 8] and was created for comparison. The stiffness values for the cable elements correspond to the C_5 values produced by the material model studies, as this value is what governs ligament fiber stiffness. (See Table 4-4)

Table 4-4: Beam model ligament parameters

Ligament	Element Type and Material Model	Material Parameters
Anterior Longitudinal	Tension-only linear cable element	E = 14.52 MPa
Interspinous		E = 20.08 MPa
Supraspinous		E = 19.24 MPa

Each applied moment increased linearly to a maximum of 7.5 N-m over a period of 560 seconds, with the exception of the lateral bending simulations, which experienced a maximum torque of 6 N-m. These loading conditions were applied to the following model configurations: a control model with no modifications, a model with updated material models, a model with updated material models and in situ strain, a model with updated material models and localized SSL properties, and a composite model with updated material models, in situ strain and localized SSL material properties. Additionally, a model with beam representations for ligaments was also

tested. This constitutes a total of 36 finite element model simulations. These simulations will henceforth be referred to as case numbers I – VI as laid out in Table 4-5.

Table 4-5: Simulation case numbers

Simulation	Case #
Control	I
Updated material models	II
Updated material models and localized SSL properties	III
Updated material models and in situ strain	IV
Updated material models, localized SSL properties model and in situ strain	V
Beam element ligaments	VI

4.2.6 Post-processing

Upon completion, data from each simulation was recorded and analyzed to isolate the desired metrics. Due to geometric near-symmetry, the results from positive and negative axial rotation and lateral bending were averaged.

Pressure inside the nucleus pulposus was obtained by recording the pressure of a sphere of elements at the center of each simulated nucleus pulposus which ranged from 3.5 to 6.5 mm in diameter according the size of the nucleus. The results across all nuclei were averaged. (See Figure 4-1)

Principal stresses, strains and shear stresses and strains were recorded from each vertebrae. These values were then used to compute strain energy (W) such that:

$$W = 0.5(\sigma_{xx}\varepsilon_{xx} + \sigma_{yy}\varepsilon_{yy} + \sigma_{zz}\varepsilon_{zz} + \sigma_{xy}\varepsilon_{xy} + \sigma_{yz}\varepsilon_{yz} + \sigma_{xz}\varepsilon_{xz}) \quad (4\text{-}7)$$

The results across all vertebrae were then averaged. (See figure 4-2)

To calculate range of motion, uniplanar lines were first drawn on the top and bottom surface of each vertebrae. These lines were oriented perpendicular to the axis of rotation. The change of angle history between the line on bottom surface of one vertebrae and the top surface of the inferior vertebrae was recorded. This process was repeated between each vertebrae and for each axis of rotation. This history data was plotted against the known torque curve for each simulation. Curves from different configurations corresponding to the same location and mode of bending were then overlaid for comparison. Range of motion was calculated as the sum of the change of angle for each vertebrae pair at the conclusion of each simulation. (See Figure 4-3)

The von Mises stress for each major spinal ligament was recorded. For ligaments spanning several vertebrae, only those elements situated between the vertebrae were measured. The results for each ligament were averaged. (See Figures 4-4 – 4-9)

4.3 Results

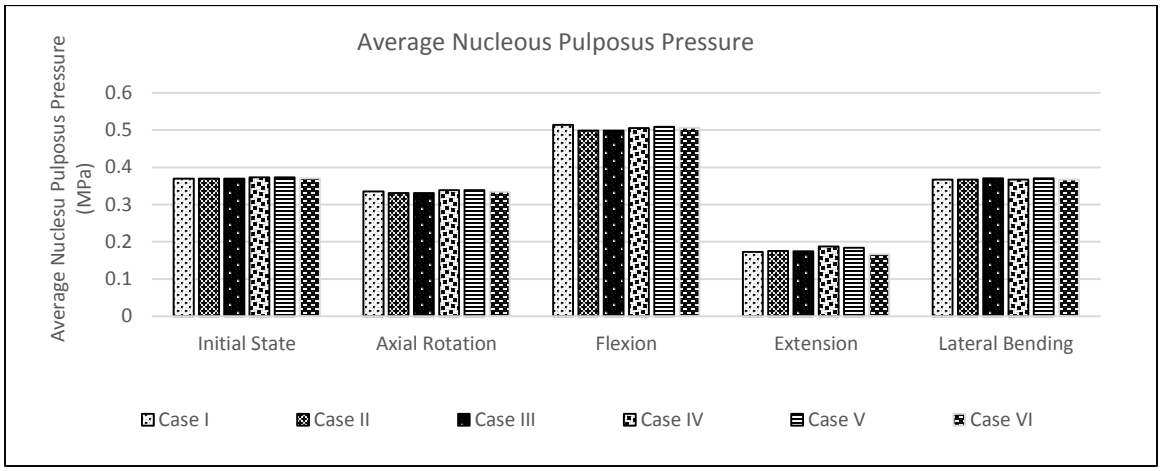

Figure 4-1: Average nucleus pulposus pressure across all discs for each case and mode of bending

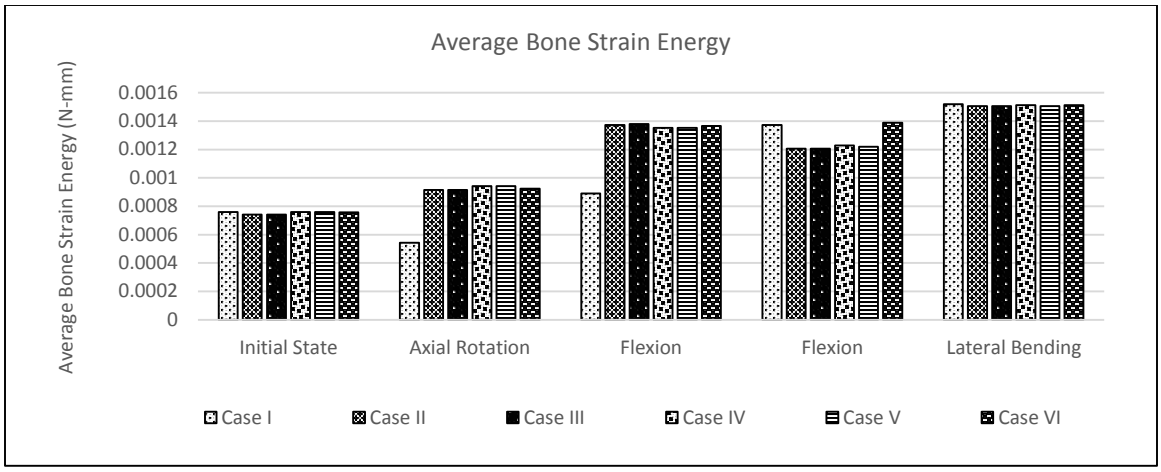

Figure 4-2: Average bone strain energy across all vertebrae for each case and mode of bending

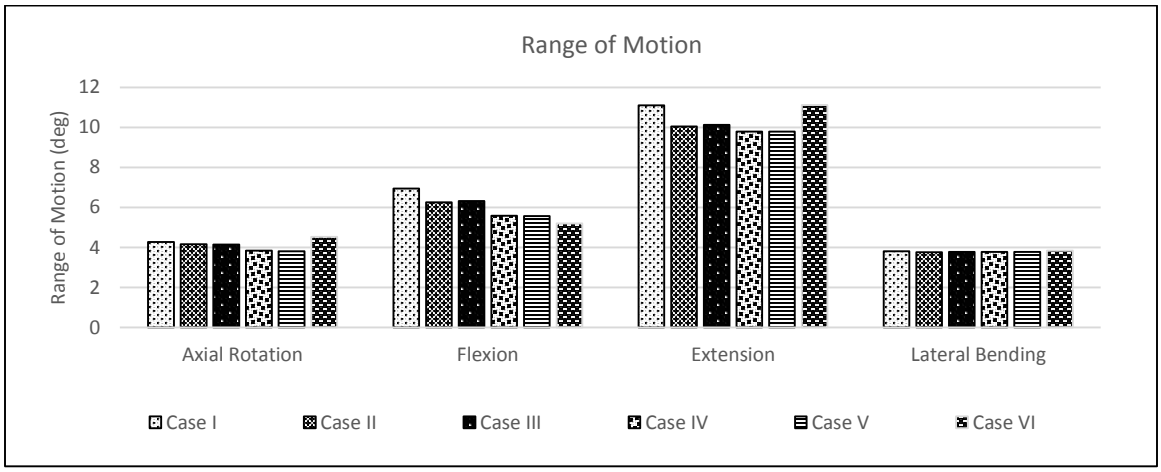

Figure 4-3: Range of motion for each case and mode of bending

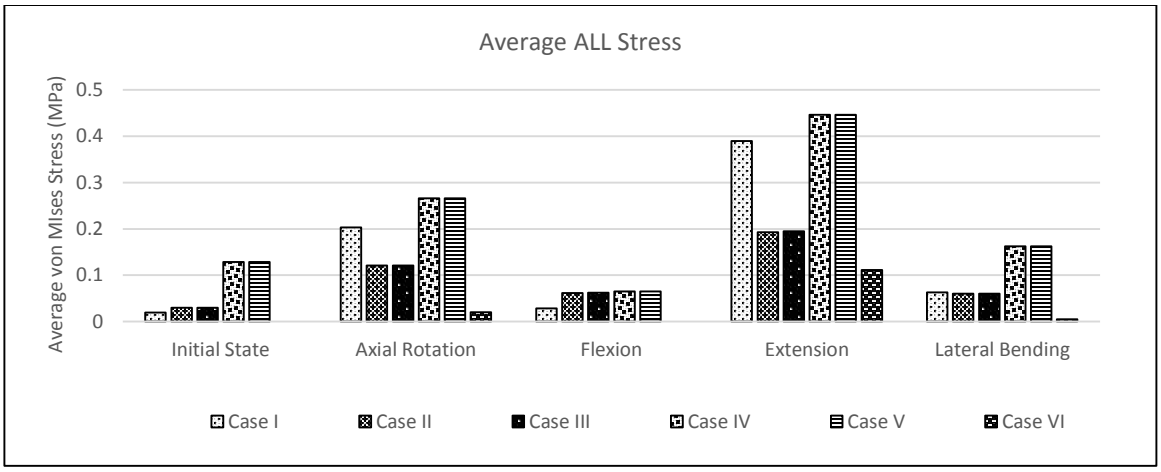

Figure 4-4: Average von Mises stress in the ALL for each case and mode of bending

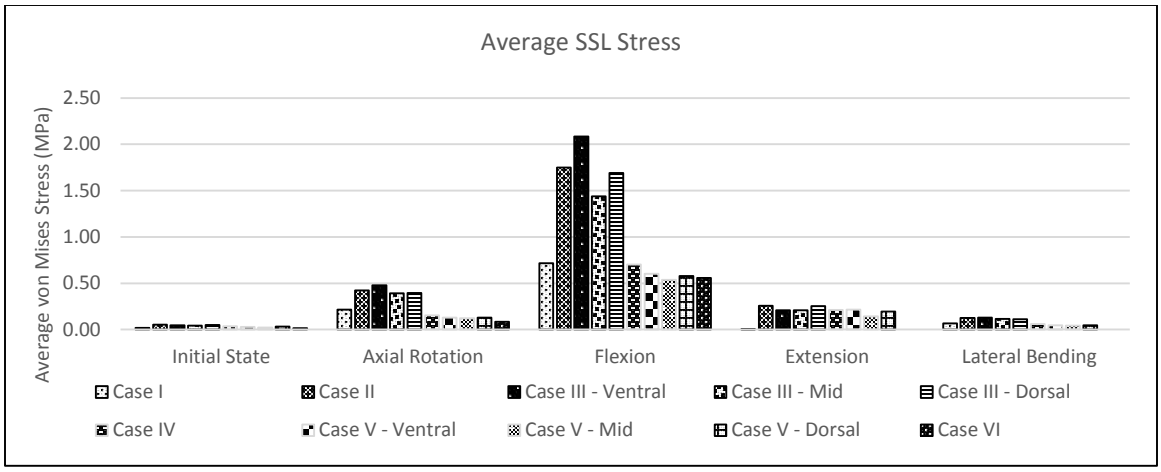

Figure 4-5: Average von Mises stress in the SSL for each case and mode of bending

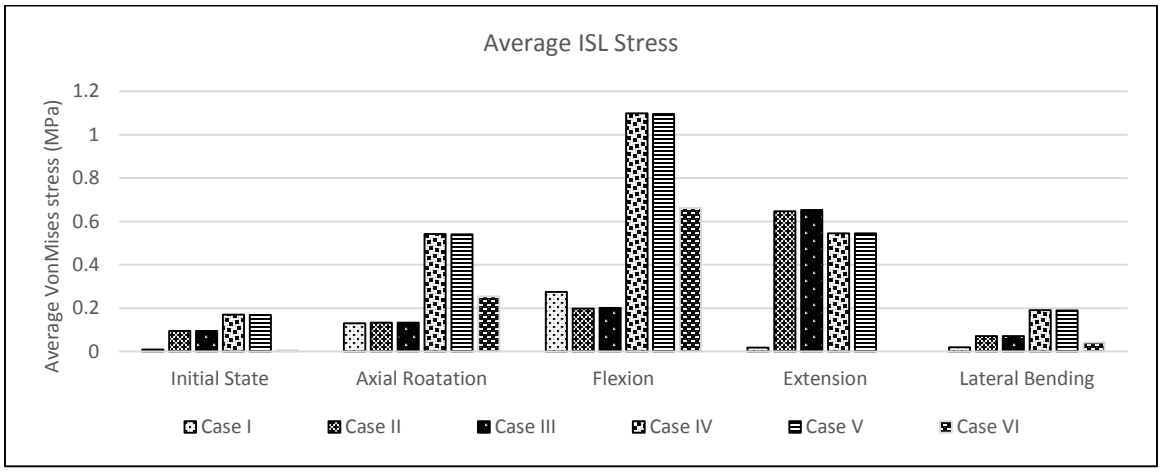

Figure 4-6: Average von Mises stress in the ISL for each case and mode of bending

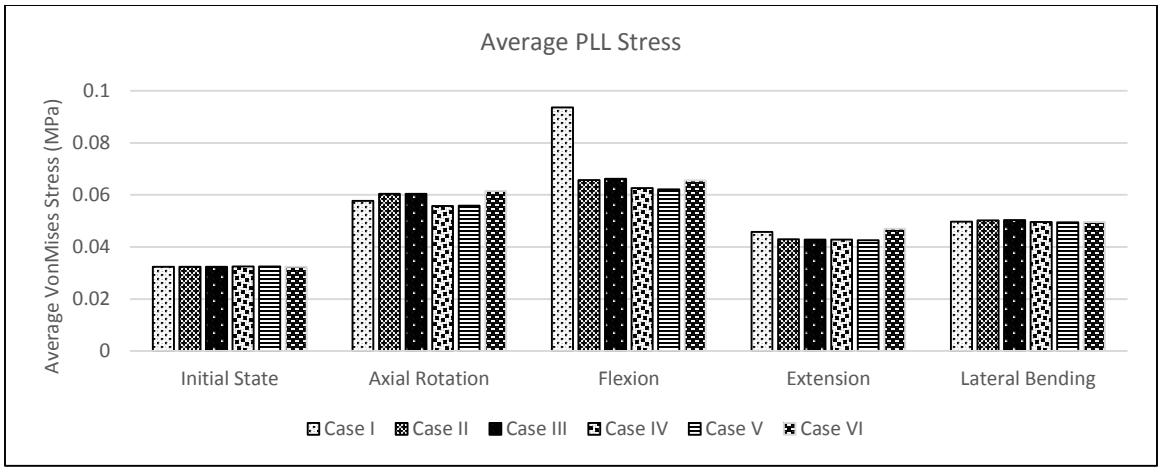

Figure 4-7: Average von Mises stress in the PLL for each case and mode of bending

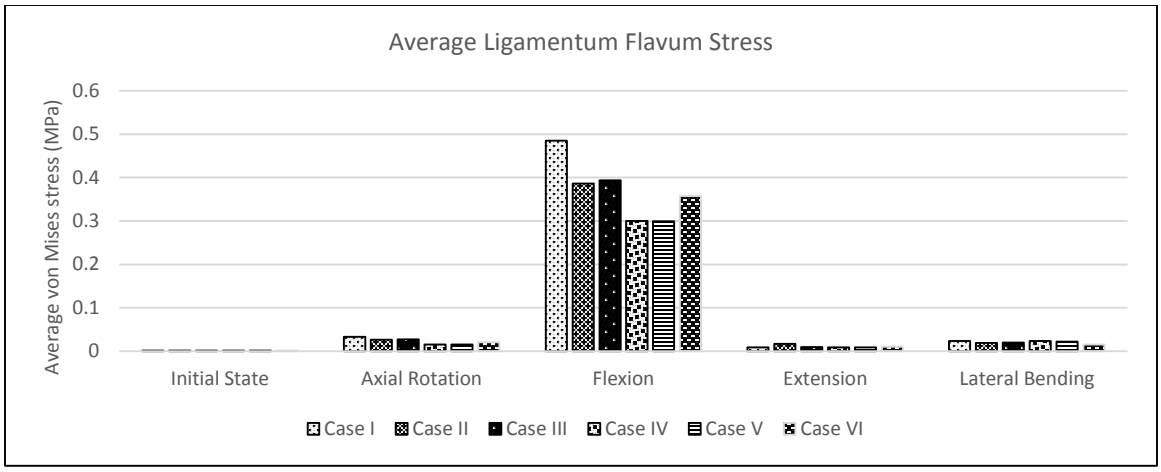

Figure 4-8: Average von Mises stress in the ligamentum flavum for each case and mode of bending

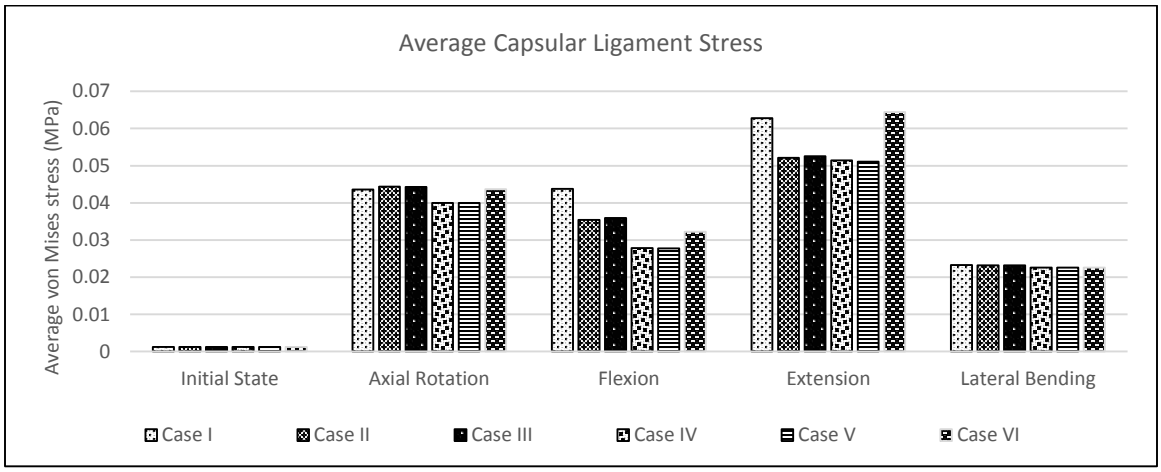

Figure 4-9: Average von Mises stress in the capsular ligaments for each case and mode of bending

4.4 Observations

The most prevalent trend seen across all result metrics is that major changes will often occur with the application of the updated material models, and then again with the application of in situ strain. With the exception of ligament stress in the SSL (Figure 4-5), the results show little difference between cases II and III, and between cases IV and V. This suggests that the effect of the application of localized SSL properties was constrained to the SLL itself.

The most extreme effects of the model modifications are seen in the ligament stresses, particularly those ligaments that were directly modified (Figures 4-4 – 4-6). Moderate differences

(< 75% change from control) are seen in bone strain energy (Figure 4-2) and range of motion (Figure 4-3), and very slight changes (<10% change from control) are seen in nucleus pressure (Figure 4-1). It should be noted that FE analysis is not subject to the external noise of physical experiments, and as such even small differences can be considered significant. However, the magnitude of these changes is relevant, and is considerably smaller than the expected ranges for inter-subject variability.

In several modes of loading, the ligament stress results for case VI (cable element ligament representation) are shown to be zero. It can be seen that these are situations where the ligament in question is being compressed rather than stretched in that mode of spinal loading. The zero stresses are due to the fact that the ligaments are modeled with tension–only cable elements that do not produce a force when in compression.

The effects of the modifications on nucleus pressure (Figure 4-1) are very slight (<10% change from control). The most dramatic effects come from case IV and V, which caused an 8.33% and 6.58% increase in disc pressure when compared to the control case. Thus we can infer that choice of FE ligament formulation has little significant effect on nucleus pressure.

Bone strain energy (Figure 4-2) sees moderate changes during axial rotation, flexion and extension. Axial rotation saw the largest increases ranging from 68.8%-73.5% when compared to the control. Bone strain energy during flexion saw increases that ranged from 52%-55%. The bone strain energy decreases in every case except case VI for extension, with decreases ranging from 10.5%-12.1%. There is little variation in bone strain energy for cases II-V suggesting that the updated material models had the greatest effect on the results, though the effect is moderate.

In each mode of bending, the control case had the highest angle of rotation (Figure 4-3). The range of motion during lateral bending was not affected, but axial rotation saw a decrease of

about 3% for cases II-III and 10% for cases IV-V. The range of motion for extension decreased by about 9% for cases II-III, and 12% for cases IV-V. Flexion saw the greatest effects due to the modifications with a range of motion decrease of 9.5% for cases II-IV and 20% for cases IV-V. This suggests that in situ strain had the greatest effect on limiting the range of motion, though the effect is moderate.

The average stress in the ALL (Figure 4-4) was significantly affected by the model modifications, especially during axial rotation and extension. Cases II-III caused a 40% decrease in ligament stress during axial rotation and a 50% decrease during extension. Cases IV-V caused a 30% increase in stress during axial rotation and a 14% increase during extension. Thus, the updated material models caused an overall decrease in ligament stress and in situ strain caused a very significant increase.

The stress in the SSL (Figure 4-5) was the only metric that saw the significant changes due to the localized SSL properties. In each case, the ventral portion of the SSL had the highest stress values, followed by the dorsal portion, then the midsection. The greatest changes were seen during extension where, cases II-III saw a significant increase (101%-191%) in SSL stress compared to the control, and cases IV-V saw a slight decrease (15%-24%). Thus, the updated material models caused an overall increase in ligament stress and in situ strain caused a subsequent decrease.

The ISL (Figure 4-6) saw the greatest changes as a result of the model modifications, especially during axial rotation, flexion and extension. During axial rotation, the ligament stress stayed constant for cases II-III and significantly increased for cases IV-V. Case VI saw a moderate increase in stress compared to the control. During flexion, there was a slight decrease in ligament stress compared to the control for cases II-III and a dramatic increase for cases IV-V. Case VI also saw a significant increase in stress. The ligament stress in extension for the control case was very

low. This metric saw significant increases for cases II-V, though cases IV-V has slightly lower stresses than cases II-III.

The other spinal ligaments that weren't directly modified (PLL, ligamentum flavum, and capsular ligaments) were also affected by the model modifications (Figures 4-7 – 4-9), though not as dramatically. For the PLL and the ligamentum flavum, the most significant changes occurred during extension where the modifications caused a decrease in ligament stress compared to the control. The capsular ligament also saw a decrease in ligament stress for cases II-V for both extension and flexion.

4.5 Discussion

Of particular interest is the comparison of the case VI with the other cases, which can be seen as a comparison of shell and beam elements. The significant differences occur in the ligament stresses of the ISL, SSL and ALL. In the ISL stresses there is a significant increase in ligament stress when compared with cases I-III. This is expected as a linear model will produce higher stress values than a nonlinear model for ligaments, especially at low levels of strain[2]. The stress values for case VI are lower than those of cases V and VI because the beam elements do not include an initial strain value. The stress values in the SSL are slightly lower for case VI than for the other cases. This is most likely due to increased load share carried by the ISL, which is coupled with the SSL[4]. The stress values in the ALL are significantly lower in case VI than the other cases. It is hypothesized that this is due to the fact that the beam elements are not influenced by bulging in the intervertebral discs. The ALL lies directly over the ventral side of the discs and as they bulge outward under load[70], they contribute to the strain in the ALL. The shell representation of the ALL captures this phenomenon while the beam representation only computes the strain from the change in distance between two points on opposing vertebrae.

The issue of most import to future FE analyses of the lumbar spine is whether or not these results warrant a change of methodology in developing FE models. One factor in this decision is the increase in computing time required to complete the FE simulations with these modifications. Figure 4-10 shows the typical CPU hours required to complete a full simulation for each case. The analyses were performed on a 12-core Intel Haswell (2.3 GHz) workstation with 64 GB of core memory. As can be seen from the figure, the composite case actually took less time than the control case, indicating that there is not a significant increase in computing time required to apply the modifications. This does not, however, capture the increase in preprocessing time required to implement these modifications. For this study, the preprocessing steps that are outlined in the methods section required approximately 30 hours for the initial set up and an additional hour in each subsequent simulation.

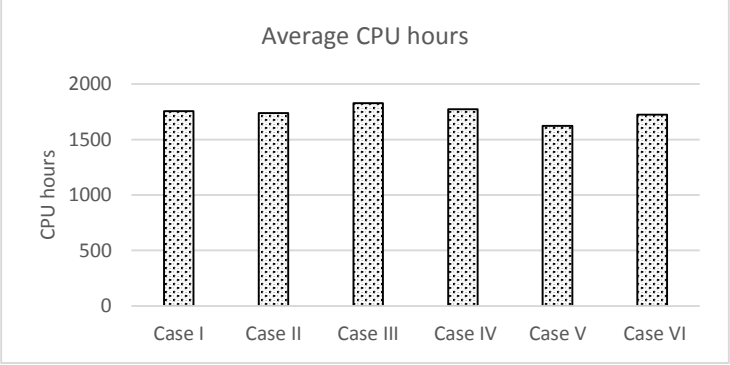

Figure 4-10: Typical CPU hours required to complete a full simulation for each case

Most clinical applications of FE analyses are concerned with strain energy in the bones as it relates to bone remodeling[1]. As the modifications made to the FE model only have a moderate impact on bone strain energy that likely lies within the range of inter-subject variability, the authors

do not recommend a change in methodology in every case. However, modifications should be considered if ligament stresses are the desired metric in an FE simulation.

The accuracy of the simulation results with respect to physical in vivo behavior is difficult to quantify. This difficulty arises from the experimental challenges of measuring quantities such as bone strain energy or disc pressure, as well as the high inter-subject variability in material properties that is typical of biological tissue. This study assumes that the inclusion of the model modifications creates a more fidelic and therefore more accurate model of spinal mechanics.

In the current study, software limitations necessitated a manual approach to applying in situ strain through the use of history variables as described in the methods section. This approach was labor intensive and the multi-step nature of the procedure provides opportunities for human error. In the present work, the process was carefully validated using small scale simulations, and the results were compared with previously published work [15]. Future studies would benefit from finding a more streamlined method to implement initial strain values that reduces the possibility for human error.

In summary, the three-dimensional, non-linear behavior of spinal ligaments has a measureable difference on lumbar spine mechanics. The application of a transversely isotropic material model and in situ strain made significant differences in measured ligament stresses. The effect of these changes on disc pressure and bone strain energy are more moderate and therefore don't necessitate a restructuring of lumbar spine FE models for most clinical applications. When ligament stresses are the desired metric however, these phenomena should be represented in order to produce realistic results.

4.6 Acknowledgements

I want to thank my coauthor Dr. Anton Bowden for his contribution to the methods, analysis and writing of this study. I also want to thank Boston Barham and Michaela Green for their help in running the simulations and data extraction.

5 SUMMARY AND FUTURE WORK

5.1 Summary of contributions

The body of research presented here provides material parameters that may be used to describe the anterior longitudinal ligament using a nonlinear, transversely isotropic material model that closely mirrors the in vivo ligament behavior. It has been shown that these parameters, in conjunction with similar results for other major spinal ligaments can used to create a high fidelity finite element model of the human lumbar spine. The inclusion of a transversely isotropic ligament material models and ligament in situ strain produces a measurable difference in disc pressure, bone strain energy, range of motion, and ligament stress when compared to a less fidelic model. These changes in ligament stress for those ligaments directly modified were the most significant.

The material parameters presented here may easily be incorporated into finite element simulations of the lumbar spine. The effects of the model changes on bone strain energy and disc pressure were moderate enough not to necessitate changes in most models that are used for clinical applications. However, future investigations on ligament stresses using finite element analysis will be able to produce more realistic results by the inclusion of these model modifications.

5.2 Topics for future work

This work includes updated material models and in situ strain data for three of the major spinal ligaments, and localized properties for one. As more experimental data becomes available,

it will be instructive to further update the finite element representation of the lumbar spine and track the changes in the resulting metrics caused by any modifications.

This work did not attempt to represent the viscoelastic properties of the ligament tissue. The transversely isotropic material model currently used can be expanded to account for this phenomenon, and the experimental methodology used here could easily be expanded investigate the effects of the inclusion of viscoelastic behavior into the finite element simulation.

REFERENCES

[1] V. C. Mow and R. Huiskes, *Basic orthopaedic biomechanics & mechano-biology*, 3rd ed. Philadelphia, PA: Lippincott Williams & Wilkins, 2005.

[2] J. A. Weiss and J. C. Gardiner, "Computational modeling of ligament mechanics," *Crit Rev Biomed Eng,* vol. 29, pp. 303-71, 2001.

[3] U. M. Ayturk and C. M. Puttlitz, "Parametric convergence sensitivity and validation of a finite element model of the human lumbar spine," *Comput Methods Biomech Biomed Engin,* vol. 14, pp. 695-705, Aug 2011.

[4] V. K. Goel and J. D. Clausen, "Prediction of load sharing among spinal components of a C5-C6 motion segment using the finite element approach," *Spine (Phila Pa 1976),* vol. 23, pp. 684-91, Mar 15 1998.

[5] D. D. Jebaseelan, C. Jebaraj, N. Yoganandan, and S. Rajasekaran, "Validation efforts and flexibilities of an eight-year-old human juvenile lumbar spine using a three-dimensional finite element model," *Med Biol Eng Comput,* vol. 48, pp. 1223-31, Dec 2010.

[6] M. B. Panzer and D. S. Cronin, "C4-C5 segment finite element model development, validation, and load-sharing investigation," *J Biomech,* vol. 42, pp. 480-90, Mar 11 2009.

[7] N. Kallemeyn, A. Gandhi, S. Kode, K. Shivanna, J. Smucker, and N. Grosland, "Validation of a C2-C7 cervical spine finite element model using specimen-specific flexibility data," *Med Eng Phys,* vol. 32, pp. 482-9, Jun 2010.

[8] J. Noailly, H. J. Wilke, J. A. Planell, and D. Lacroix, "How does the geometry affect the internal biomechanics of a lumbar spine bi-segment finite element model? Consequences on the validation process," *J Biomech,* vol. 40, pp. 2414-25, 2007.

[9] J. A. Wheeldon, B. D. Stemper, N. Yoganandan, and F. A. Pintar, "Validation of a finite element model of the young normal lower cervical spine," *Ann Biomed Eng,* vol. 36, pp. 1458-69, Sep 2008.

[10] J. S. Wu and J. H. Chen, "Clarification of the mechanical behaviour of spinal motion segments through a three-dimensional poroelastic mixed finite element model," *Med Eng Phys,* vol. 18, pp. 215-24, Apr 1996.

[11] H. Zhang and J. Bai, "Nonlinear finite element analysis of C0-C1-C2 complex under physiologic loads," *Conf Proc IEEE Eng Med Biol Soc,* vol. 6, pp. 6165-7, 2005.

[12] H. S. Park, C. Ahn, D. T. Fung, Y. Ren, and L. Q. Zhang, "A knee-specific finite element analysis of the human anterior cruciate ligament impingement against the femoral intercondylar notch," *J Biomech,* vol. 43, pp. 2039-42, Jul 20 2010.

[13] F. Xie, L. Yang, L. Guo, Z. J. Wang, and G. Dai, "A study on construction three-dimensional nonlinear finite element model and stress distribution analysis of anterior cruciate ligament," *J Biomech Eng,* vol. 131, p. 121007, Dec 2009.

[14] N. M. Lalonde, Y. Petit, C. E. Aubin, E. Wagnac, and P. J. Arnoux, "Method to geometrically personalize a detailed finite-element model of the spine," *IEEE Trans Biomed Eng,* vol. 60, pp. 2014-21, Jul 2013.

[15] D. J. Robertson, G. A. Von Forell, J. Alsup, and A. E. Bowden, "Thoracolumbar spinal ligaments exhibit negative and transverse pre-strain," *J Mech Behav Biomed Mater,* vol. 23, pp. 44-52, Jul 2013.

[16] J. A. Weiss, J. C. Gardiner, B. J. Ellis, T. J. Lujan, and N. S. Phatak, "Three-dimensional finite element modeling of ligaments: technical aspects," *Med Eng Phys,* vol. 27, pp. 845-61, Dec 2005.

[17] A. M. Sadegh and A. Tchako, "Vertebral stress of a cervical spine model under dynamic load," *Technol Health Care,* vol. 8, pp. 143-54, 2000.

[18] D. P. Pioletti, L. R. Rakotomanana, J. F. Benvenuti, and P. F. Leyvraz, "Viscoelastic constitutive law in large deformations: application to human knee ligaments and tendons," *J Biomech,* vol. 31, pp. 753-7, Aug 1998.

[19] M. A. Puso and J. A. Weiss, "Finite element implementation of anisotropic quasi-linear viscoelasticity using a discrete spectrum approximation," *J Biomech Eng,* vol. 120, pp. 62-70, Feb 1998.

[20] L. Dong, G. Li, H. Mao, S. Marek, and K. H. Yang, "Development and validation of a 10-year-old child ligamentous cervical spine finite element model," *Ann Biomed Eng,* vol. 41, pp. 2538-52, Dec 2013.

[21] F. Ezquerro, F. Garcia Vacas, S. Postigo, M. Prado, and A. Simon, "Calibration of the finite element model of a lumbar functional spinal unit using an optimization technique based on differential evolution," *Med Eng Phys,* vol. 33, pp. 89-95, Jan 2011.

[22] E. C. Teo and H. W. Ng, "Evaluation of the role of ligaments, facets and disc nucleus in lower cervical spine under compression and sagittal moments using finite element method," *Med Eng Phys,* vol. 23, pp. 155-64, Apr 2001.

[23] D. Robertson, R. Willardson, D. Parajuli, A. Cannon, and A. E. Bowden, "The lumbar supraspinous ligament demonstrates increased material stiffness and strength on its ventral aspect," *J Mech Behav Biomed Mater,* vol. 17, pp. 34-43, Jan 2013.

[24] T. J. Momersteeg, L. Blankevoort, R. Huiskes, J. G. Kooloos, J. M. Kauer, and J. C. Hendriks, "The effect of variable relative insertion orientation of human knee bone-ligament-bone complexes on the tensile stiffness," *J Biomech,* vol. 28, pp. 745-52, Jun 1995.

[25] L. Blankevoort, J. H. Kuiper, R. Huiskes, and H. J. Grootenboer, "Articular contact in a three-dimensional model of the knee," *J Biomech,* vol. 24, pp. 1019-31, 1991.

[26] T. J. Mommersteeg, L. Blankevoort, R. Huiskes, J. G. Kooloos, and J. M. Kauer, "Characterization of the mechanical behavior of human knee ligaments: a numerical-experimental approach," *J Biomech,* vol. 29, pp. 151-60, Feb 1996.

[27] W. Mesfar and A. Shirazi-Adl, "Biomechanics of changes in ACL and PCL material properties or prestrains in flexion under muscle force-implications in ligament reconstruction," *Comput Methods Biomech Biomed Engin,* vol. 9, pp. 201-9, Aug 2006.

[28] R. Shirazi and A. Shirazi-Adl, "Analysis of partial meniscectomy and ACL reconstruction in knee joint biomechanics under a combined loading," *Clin Biomech (Bristol, Avon),* vol. 24, pp. 755-61, Nov 2009.

[29] L. H. Yahia and G. Drouin, "Study of the hysteresis phenomenon in canine anterior cruciate ligaments," *J Biomed Eng,* vol. 12, pp. 57-62, Jan 1990.

[30] D. W. Hukins, M. C. Kirby, T. A. Sikoryn, R. M. Aspden, and A. J. Cox, "Comparison of structure, mechanical properties, and functions of lumbar spinal ligaments," *Spine (Phila Pa 1976),* vol. 15, pp. 787-95, Aug 1990.

[31] M. K. Kwan, T. H. Lin, and S. L. Woo, "On the viscoelastic properties of the anteromedial bundle of the anterior cruciate ligament," *J Biomech,* vol. 26, pp. 447-52, Apr-May 1993.

[32] K. M. Quapp and J. A. Weiss, "Material characterization of human medial collateral ligament," *J Biomech Eng,* vol. 120, pp. 757-63, Dec 1998.

[33] F. A. Pintar, N. Yoganandan, T. Myers, A. Elhagediab, and A. Sances, Jr., "Biomechanical properties of human lumbar spine ligaments," *J Biomech,* vol. 25, pp. 1351-6, Nov 1992.

[34] J. B. Myklebust, F. Pintar, N. Yoganandan, J. F. Cusick, D. Maiman, T. J. Myers*, et al.*, "Tensile strength of spinal ligaments," *Spine (Phila Pa 1976),* vol. 13, pp. 526-31, May 1988.

[35] M. S. Sacks, "A method for planar biaxial mechanical testing that includes in-plane shear," *J Biomech Eng,* vol. 121, pp. 551-5, Oct 1999.

[36] P. M. Nielsen, P. J. Hunter, and B. H. Smaill, "Biaxial testing of membrane biomaterials: testing equipment and procedures," *J Biomech Eng,* vol. 113, pp. 295-300, Aug 1991.

[37] M. A. Cox, N. J. Driessen, R. A. Boerboom, C. V. Bouten, and F. P. Baaijens, "Mechanical characterization of anisotropic planar biological soft tissues using finite indentation: experimental feasibility," *J Biomech,* vol. 41, pp. 422-9, 2008.

[38] R. J. Bradshaw, Russell, Alison C., Bowden, Anton E, "Spinal Ligaments: Anisotropic Characterization Using Very Small Samples," *Experimental and Applied Mechanics,* vol. 6, pp. 429-436, 2011.

[39] D. J. Riemersa and H. C. Schamhardt, "The cryo-jaw, a clamp designed for in vitro rheology studies of horse digital flexor tendons," *J Biomech,* vol. 15, pp. 619-20, 1982.

[40] N. A. Sharkey, T. S. Smith, and D. C. Lundmark, "Freeze clamping musculo-tendinous junctions for in vitro simulation of joint mechanics," *J Biomech,* vol. 28, pp. 631-5, May 1995.

[41] T. P. Andriacchi, R. P. Mikosz, S. J. Hampton, and J. O. Galante, "Model studies of the stiffness characteristics of the human knee joint," *J Biomech,* vol. 16, pp. 23-9, 1983.

[42] J. R. Matyas, M. G. Anton, N. G. Shrive, and C. B. Frank, "Stress governs tissue phenotype at the femoral insertion of the rabbit MCL," *J Biomech,* vol. 28, pp. 147-57, Feb 1995.

[43] N. J. Giori, G. S. Beaupre, and D. R. Carter, "Cellular shape and pressure may mediate mechanical control of tissue composition in tendons," *J Orthop Res,* vol. 11, pp. 581-91, Jul 1993.

[44] A. Hohmann, C. Kober, P. Young, C. Dorow, M. Geiger, A. Boryor*, et al.*, "Influence of different modeling strategies for the periodontal ligament on finite element simulation results," *Am J Orthod Dentofacial Orthop,* vol. 139, pp. 775-83, Jun 2011.

[45] J. C. Gardiner and J. A. Weiss, "Subject-specific finite element analysis of the human medial collateral ligament during valgus knee loading," *J Orthop Res,* vol. 21, pp. 1098-106, Nov 2003.

[46] E. Ibarz, A. Herrera, Y. Mas, J. Rodriguez-Vela, J. Cegonino, S. Puertolas*, et al.*, "Development and kinematic verification of a finite element model for the lumbar spine: application to disc degeneration," *Biomed Res Int,* vol. 2013, p. 705185, 2013.

[47] S. Martelli, A. Joukhadar, S. Zaffagnini, R. Marcacci, S. Lavallee, and G. Champleboux, "Fiber-based anterior cruciate ligament model for biomechanical simulations," *Journal of Orthopaedic Research,* vol. 16, pp. 379-385, May 1998.

[48] J. A. Weiss, B. N. Maker, and S. Govindjee, "Finite element implementation of incompressible, transversely isotropic hyperelasticity," *Computer Methods in Applied Mechanics and Engineering,* vol. 135, pp. 107-128, 8/15/ 1996.

[49] T. J. R. Hughes and W. K. Liu, "Non-Linear Finite-Element Analysis of Shells .1. 3-Dimensional Shells," *Computer Methods in Applied Mechanics and Engineering,* vol. 26, pp. 331-362, 1981.

[50] B. J. Ellis, R. E. Debski, S. M. Moore, P. J. McMahon, and J. A. Weiss, "Methodology and sensitivity studies for finite element modeling of the inferior glenohumeral ligament complex," *J Biomech,* vol. 40, pp. 603-12, 2007.

[51] A. E. Bowden, "Finite Element Modeling of the Spine," in *Spine Technology Handbook*, S. M. Kurtx, Ed., ed Burlignton, MA: Academic Press, 2006.

[52] G. A. Von Forell and A. E. Bowden, "Biomechanical implications of lumbar spinal ligament transection," *Comput Methods Biomech Biomed Engin,* Mar 12 2013.

[53] J. V. Seligman, S. D. Gertzbein, M. Tile, and A. Kapasouri, "Computer analysis of spinal segment motion in degenerative disc disease with and without axial loading," *Spine (Phila Pa 1976),* vol. 9, pp. 566-73, Sep 1984.

[54] A. A. White and M. M. Panjabi, *Clinical biomechanics of the spine*, 2nd ed. Philadelphia: Lippincott, 1990.

[55] R. J. Bradshaw, "Mechanical characterization of the human interspinous ligament using anisotropic small punch testing," M.S., Department of Mechanical Engineering, Brigham Young University, Provo Utah, 2011.

[56] P. Neumann, T. S. Keller, L. Ekstrom, L. Perry, T. H. Hansson, and D. M. Spengler, "Mechanical properties of the human lumbar anterior longitudinal ligament," *J Biomech,* vol. 25, pp. 1185-94, Oct 1992.

[57] N. Yoganandan, S. Kumaresan, and F. A. Pintar, "Geometric and mechanical properties of human cervical spine ligaments," *J Biomech Eng,* vol. 122, pp. 623-9, Dec 2000.

[58] M. S. Sacks, "Biaxial mechanical evaluation of planar biological materials," *Journal of Elasticity,* vol. 61, pp. 199-246, 2000.

[59] D. C. Robertson, Douglas, "Unrealistic statistics: How average consitutive coefficients can produce non-physical results," *Journal of the Mechancial Behavior of Biomedical Materials,* vol. In Press, 2014.

[60] J. Chazal, A. Tanguy, M. Bourges, G. Gaurel, G. Escande, M. Guillot*, et al.*, "Biomechanical properties of spinal ligaments and a histological study of the supraspinal ligament in traction," *J Biomech,* vol. 18, pp. 167-76, 1985.

[61] L. O. Marchi, L, Coutinho, E; Pimenta L, "The importance of the anterior longitudinal ligament in lumber disc arthroplasty: 36-month follow-up experience in extreme lateral total disc replacement," *The International Journal of Spine Surgery,* vol. 6, pp. 18-23, 2012.

[62] H. Schmidt, F. Galbusera, A. Rohlmann, T. Zander, and H. J. Wilke, "Effect of multilevel lumbar disc arthroplasty on spine kinematics and facet joint loads in flexion and extension: a finite element analysis," *Eur Spine J,* vol. 21 Suppl 5, pp. S663-74, Jun 2012.

[63] I. Erdem, E. Truumees, and M. C. van der Meulen, "Simulation of the behaviour of the L1 vertebra for different material properties and loading conditions," *Comput Methods Biomech Biomed Engin,* vol. 16, pp. 736-46, 2013.

[64] S. H. Chen, C. L. Tai, C. Y. Lin, P. H. Hsieh, and W. P. Chen, "Biomechanical comparison of a new stand-alone anterior lumbar interbody fusion cage with established fixation techniques - a three-dimensional finite element analysis," *BMC Musculoskelet Disord,* vol. 9, p. 88, 2008.

[65] E. Charriere, F. Sirey, and P. K. Zysset, "A finite element model of the L5-S1 functional spinal unit: development and comparison with biomechanical tests in vitro," *Comput Methods Biomech Biomed Engin,* vol. 6, pp. 249-61, Aug 2003.

[66] A. M. Kiapour, Kaul, V., Kiapour, A., Quatman, C.E., Wordeman, S.C., Hewett, T.E., Demetropoulos, C.K., Goel, V.K., "The Effect of Ligament Modeling Technique on Knee Joint Kinematics: A Finite Element Study," *Applied Mathematics,* vol. 4, pp. 91-97, 2013.

[67] A. Shirazi-Adl and K. E. Moglo, "Effect of changes in cruciate ligaments pretensions on knee joint laxity and ligament forces," *Comput Methods Biomech Biomed Engin,* vol. 8, pp. 17-24, Feb 2005.

[68] M. Hortin, S. Graham, K. Boatwright, P. Hyoung, and A. Bowden, "Transversely isotropic material characterization of the human anterior longitudinal ligament," *J Mech Behav Biomed Mater,* vol. 45C, pp. 75-82, Feb 7 2015.

[69] S. M. Moore, P. J. McMahon, and R. E. Debski, "Bi-directional mechanical properties of the axillary pouch of the glenohumeral capsule: implications for modeling and surgical repair," *J Biomech Eng,* vol. 126, pp. 284-8, Apr 2004.

[70] P. Brinckmann, W. Frobin, E. Hierholzer, and M. Horst, "Deformation of the vertebral end-plate under axial loading of the spine," *Spine (Phila Pa 1976),* vol. 8, pp. 851-6, Nov-Dec 1983.

APPENDIX A. LIGAMENT STRESS RESULTS

The following section show the ligament stress results at each level of the spine for the ligaments that were directly modified.

A.1 Anterior longitudinal ligament

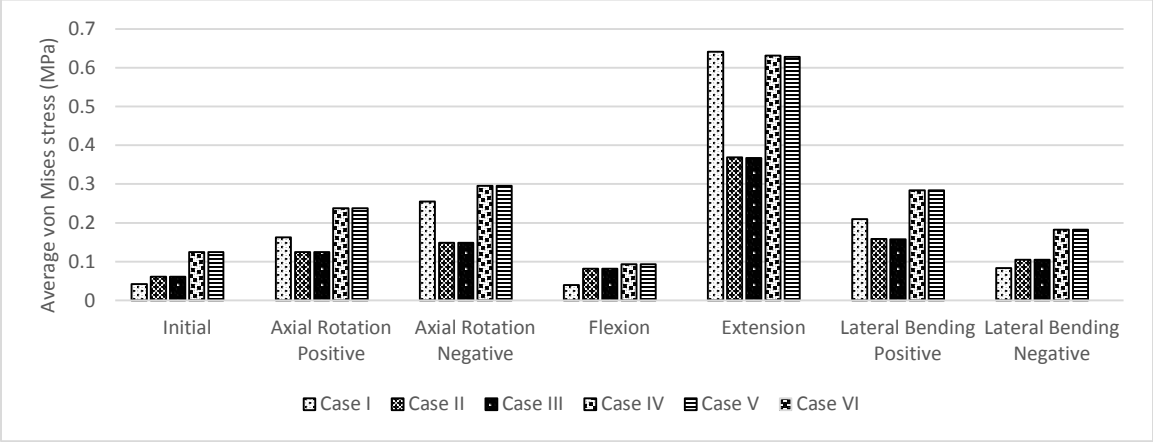

Figure A--1: Average ALL von Mises Stress in T12-L1

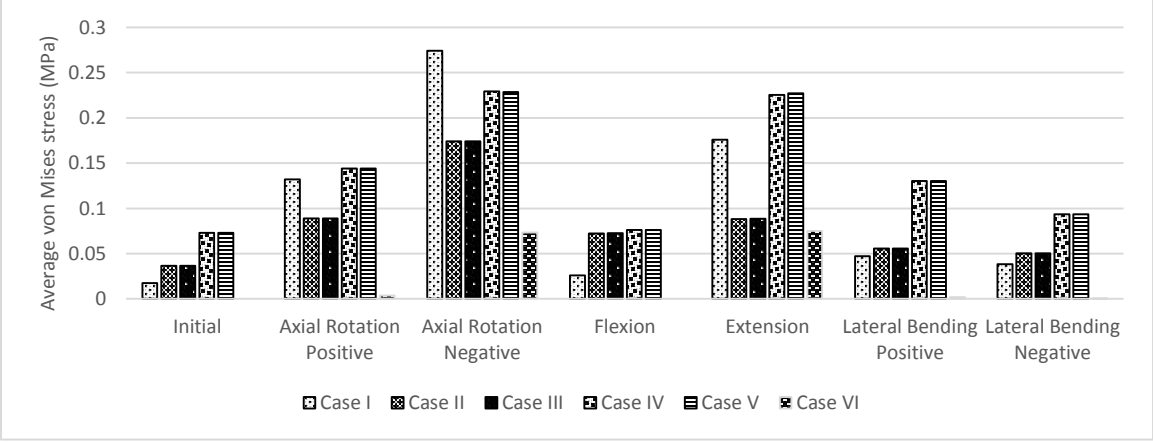

Figure A--2: Average ALL von Mises Stress in L1-L2

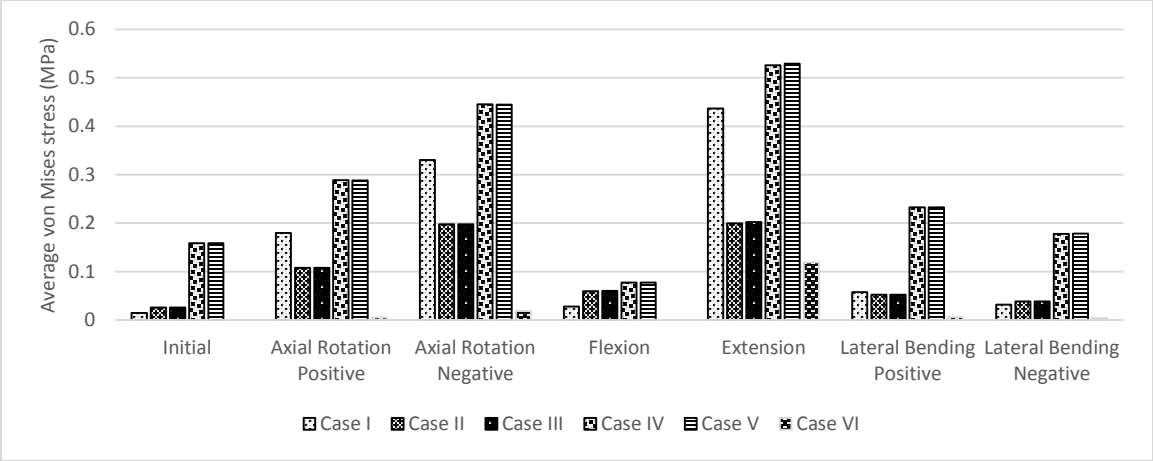

Figure A--3: Average ALL von Mises Stress in L2-L3

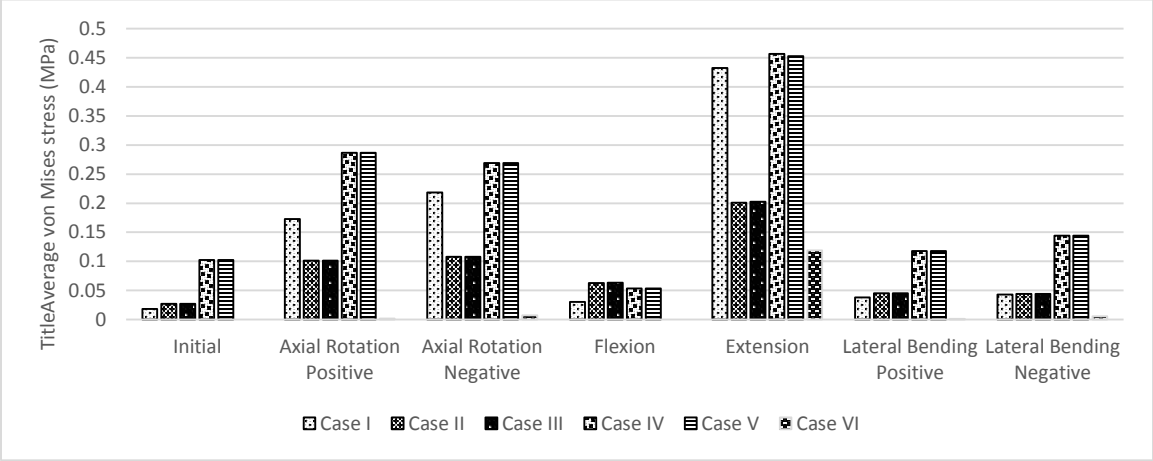

Figure A--4: Average ALL von Mises stress in L3-L4

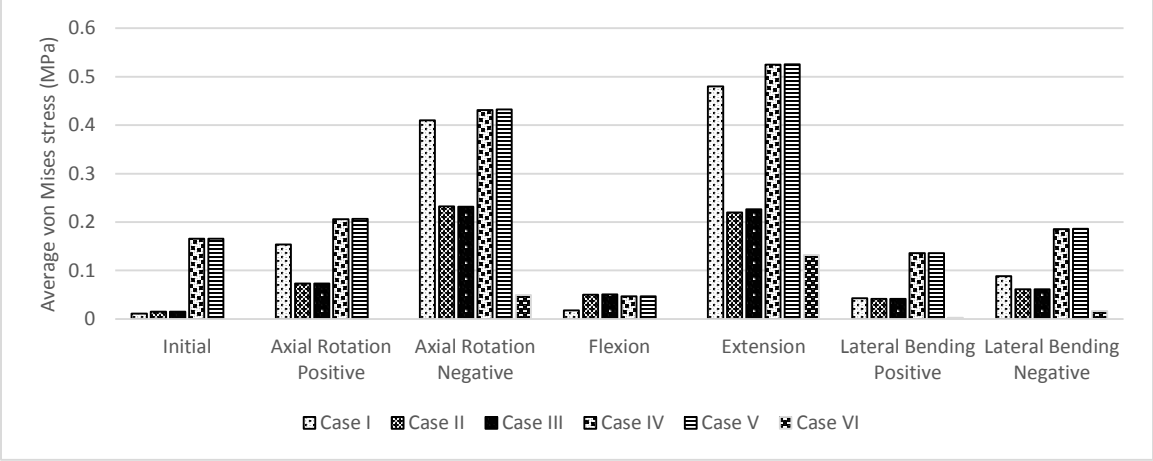

Figure A--5: Average ALL von Mises stress in L4-L5

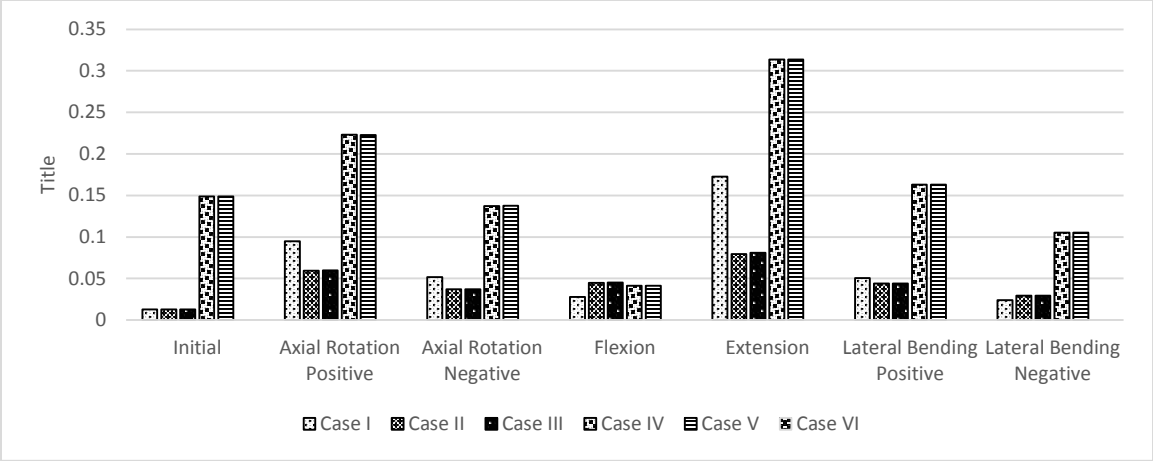

Figure A--6: Average ALL von Mises stress in L5-S1

A.2 Supraspinous ligament

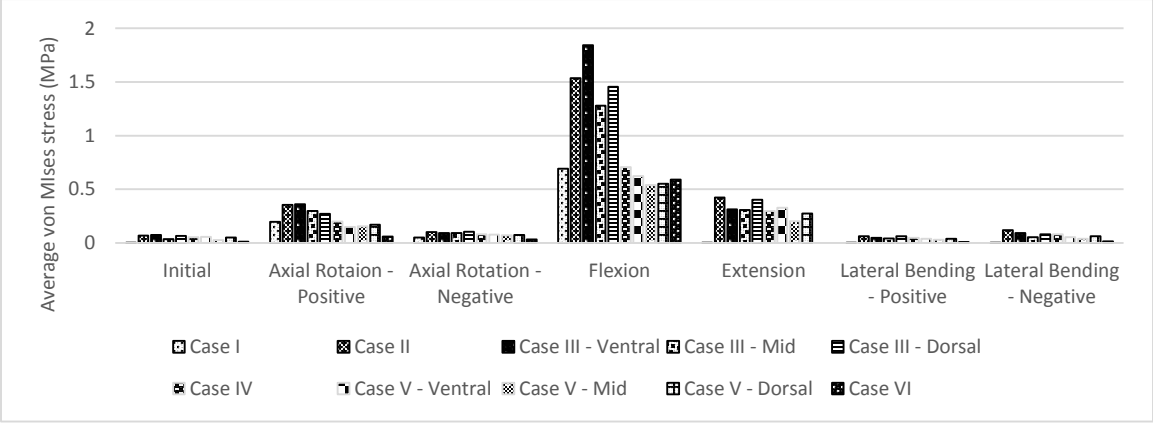

Figure A--7: Average SSL von Mises stress in T12-L1

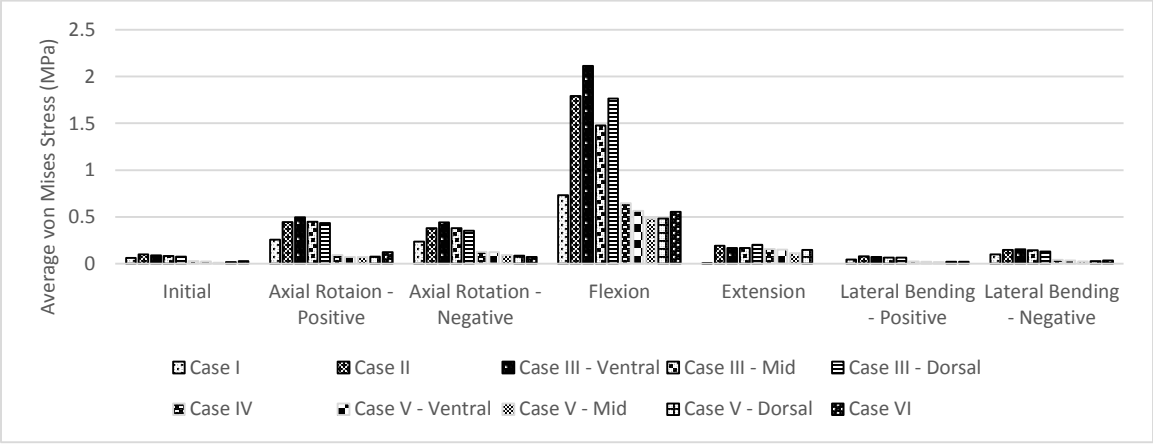

Figure A--8: Average SSL von Mises stress in L1-L2

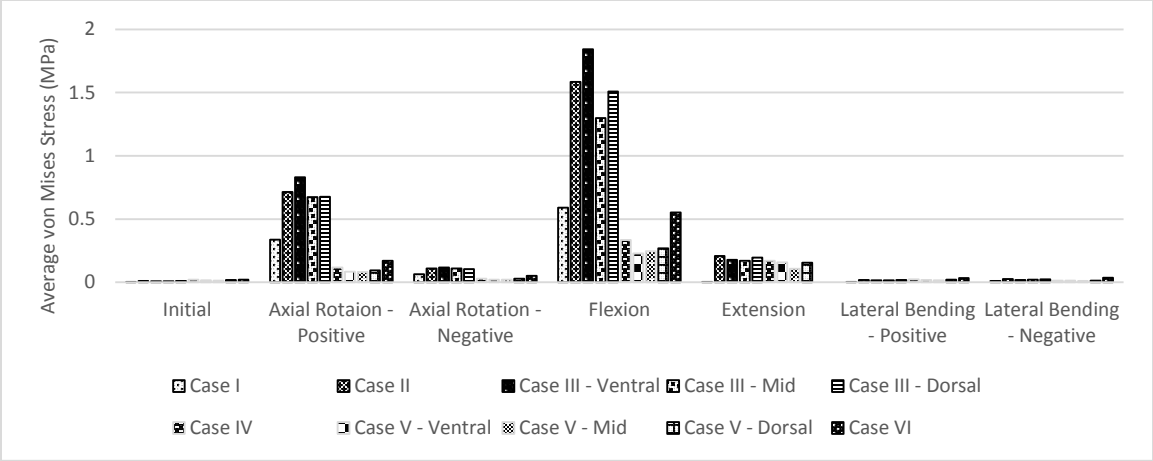

Figure A--9: Average SSL von Mises stress in L2-L3

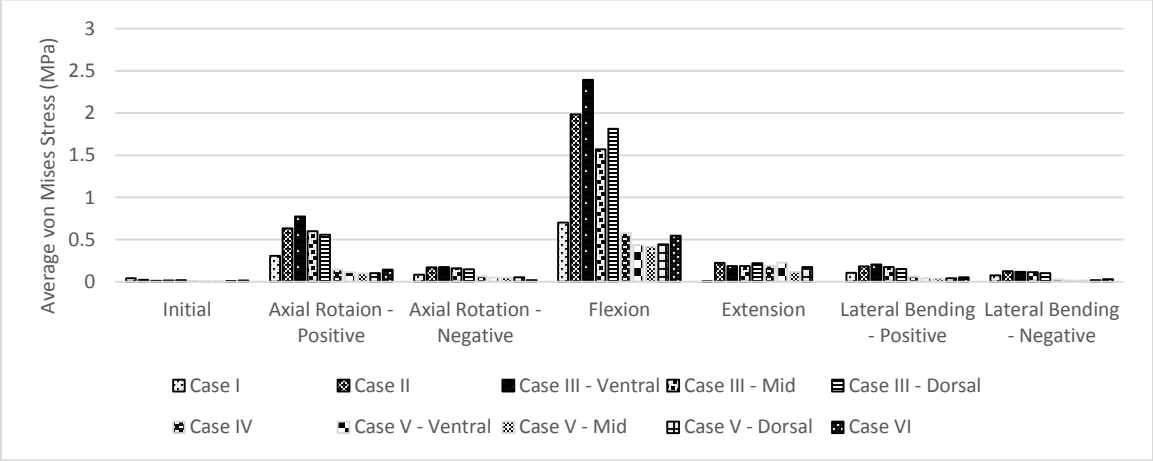

Figure A--10: Average SSL von Mises stress in L3-L4

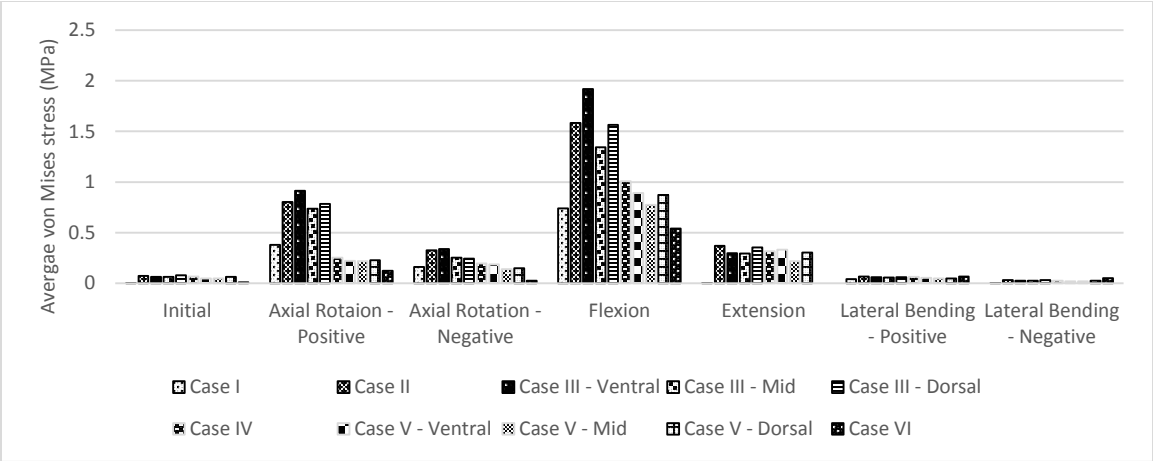

Figure A--11: Average SSL von Mises stress in L4-L5

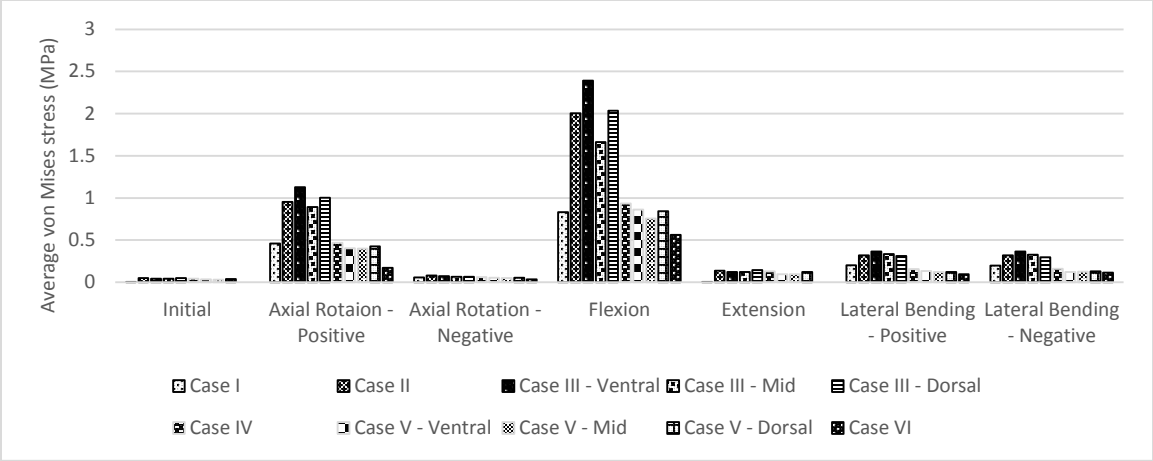

Figure A--12: Average SSL von Mises stress in L5-S1

A.3 Interspinous ligament

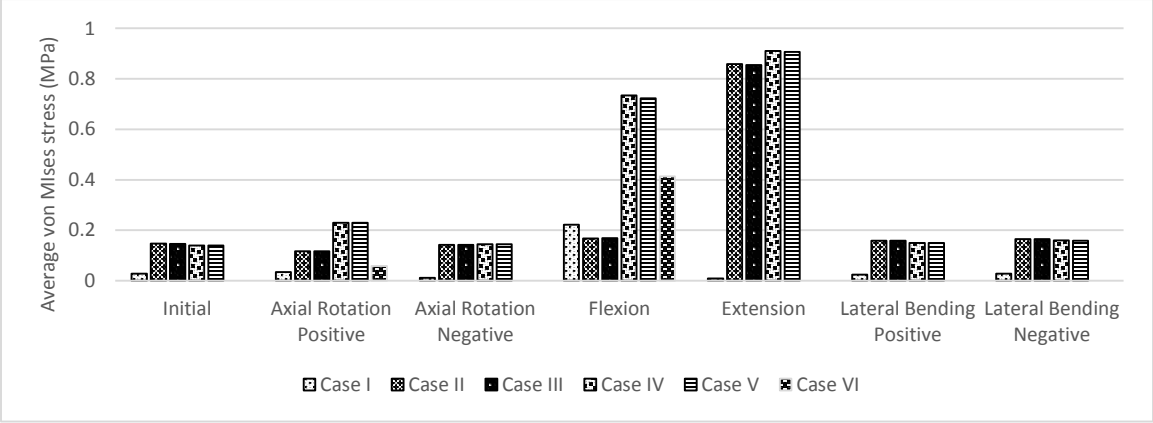

Figure A--13: Average ISL von Mises stress in T12-L1

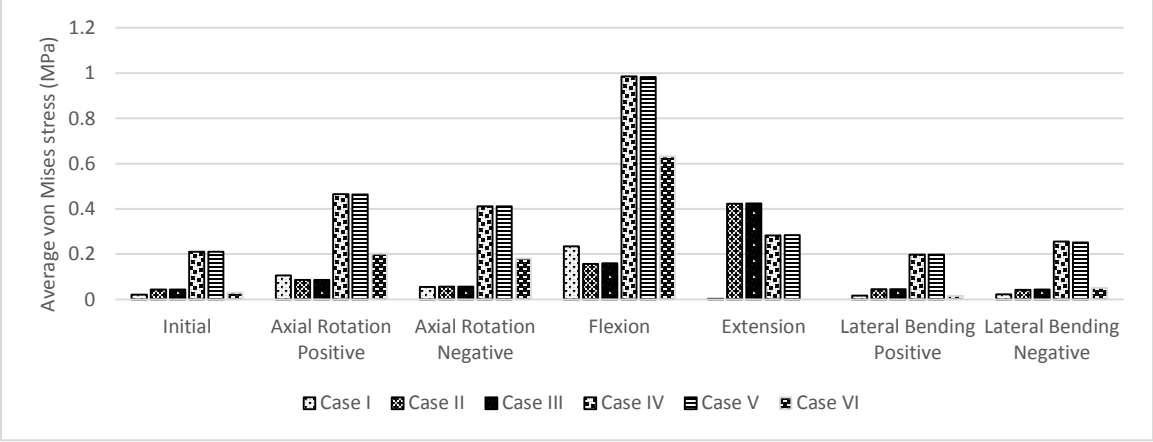

Figure A--14: Average ISL von Mises stress in L1-L2

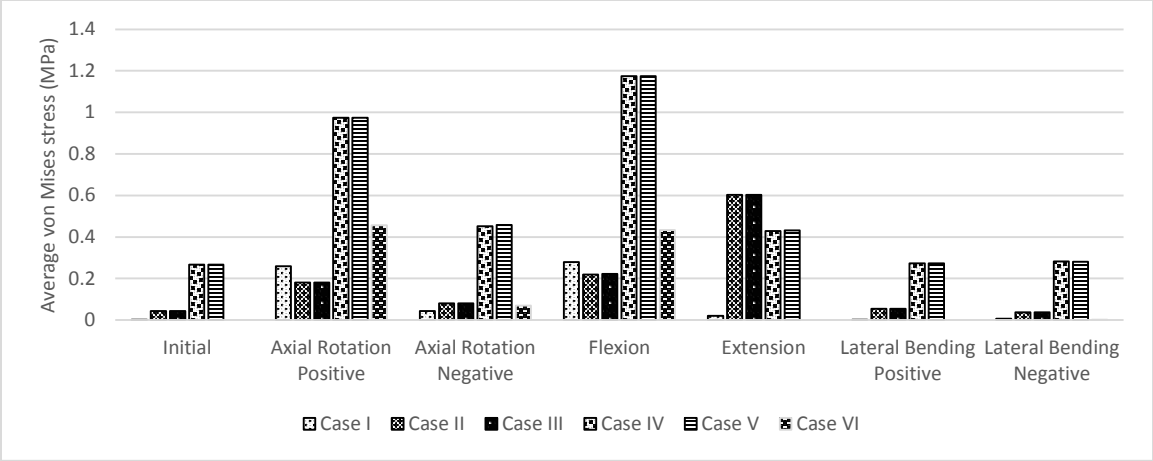

Figure A--15: Average ISL von Mises stress in L2-L3

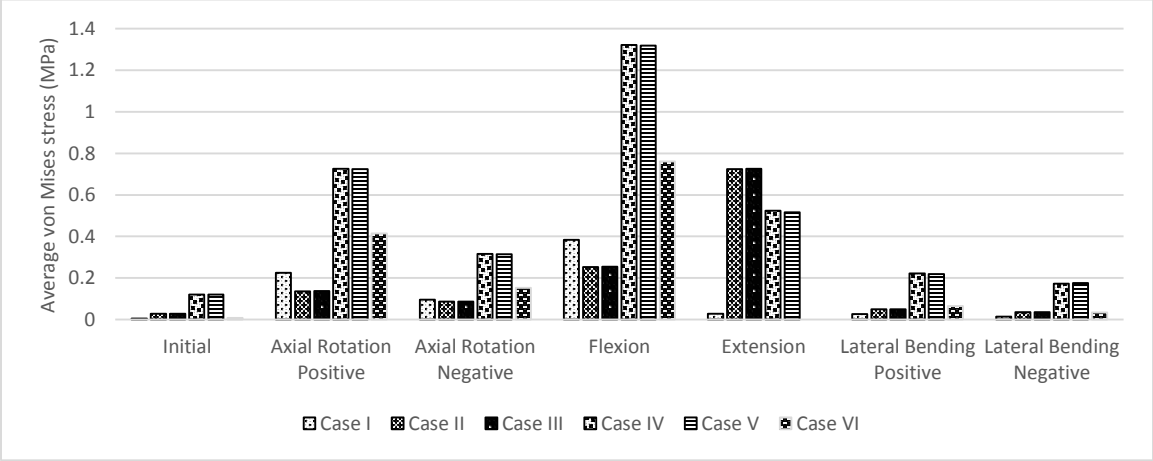

Figure A--16: Average ISL von Mises stress in L3-L4

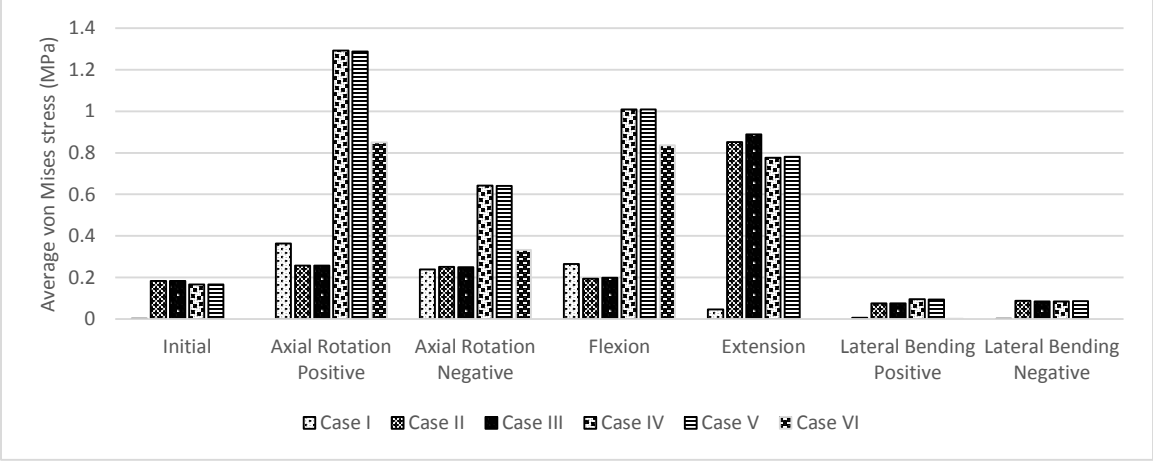

Figure A--17: Average ISL von Mises stress in L4-L5

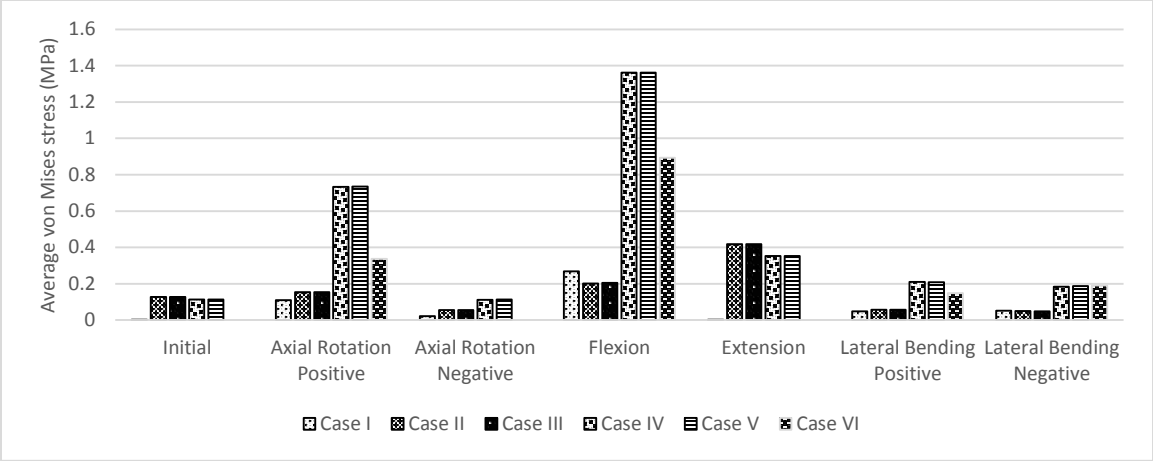

Figure A--18: Average ISL von Mises stress in L5-S1

APPENDIX B. NUCLEUS PULPOSUS PRESSURE RESULTS

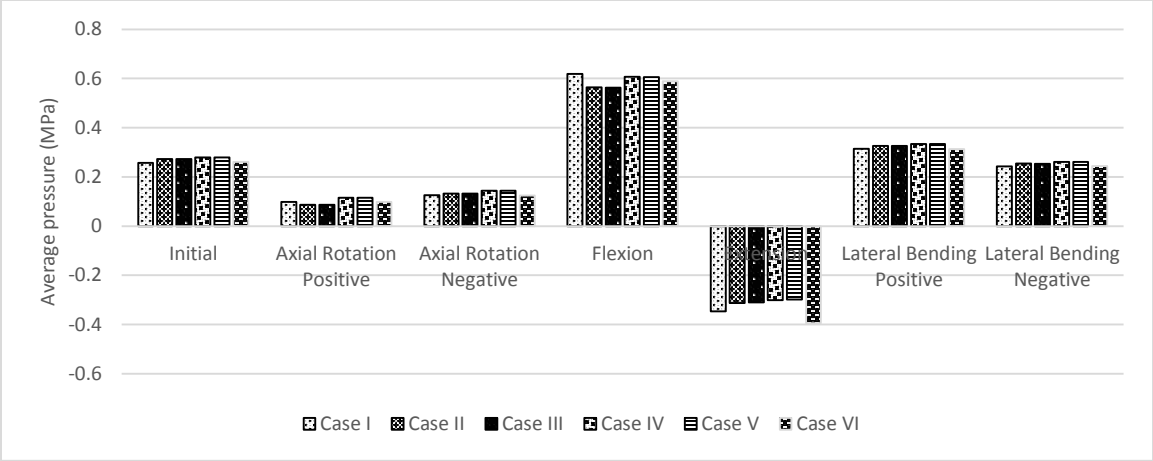

Figure B--1: Average nucleus pulposus pressure in T12-L1

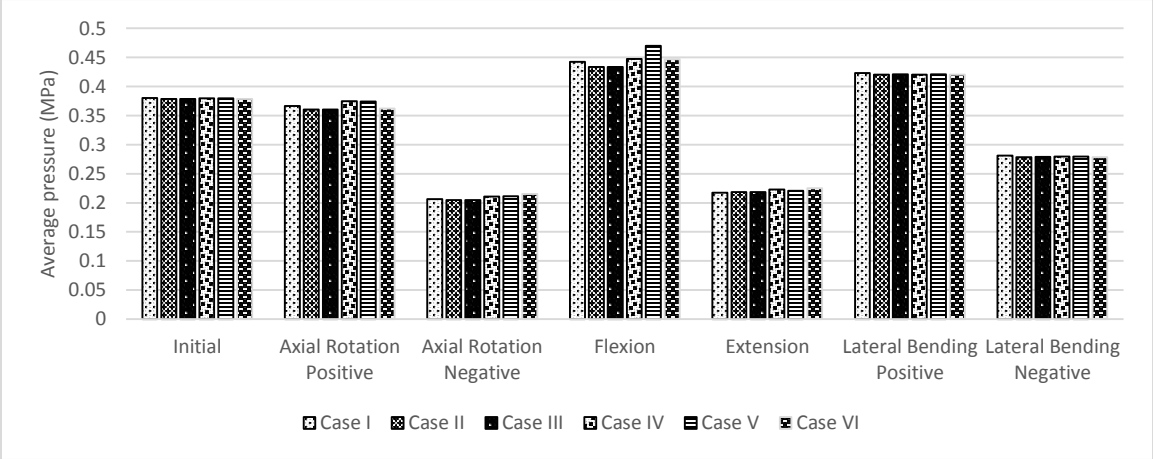

Figure B--2: Average nucleus pulposus pressure in L1-L2

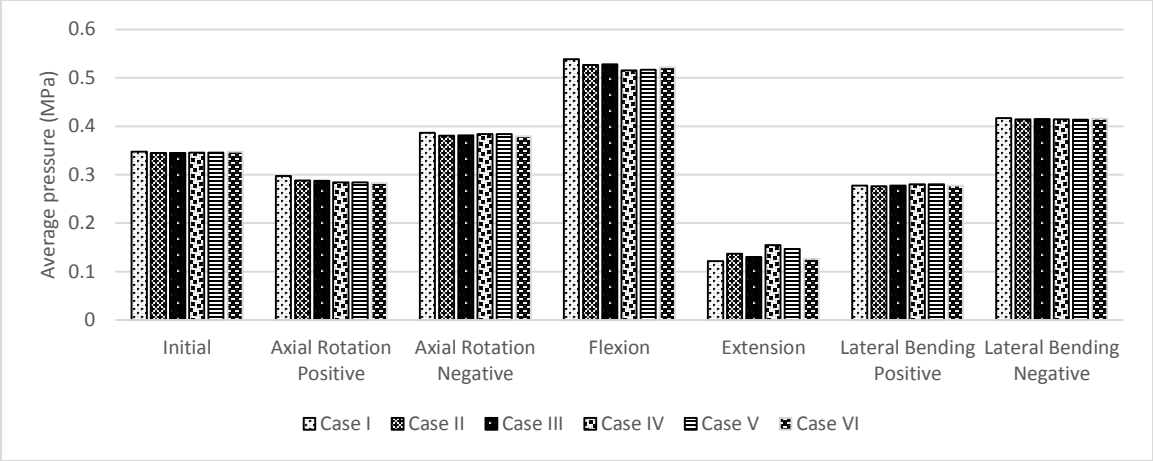

Figure B--3: Average nucleus pulposus in L2-L3

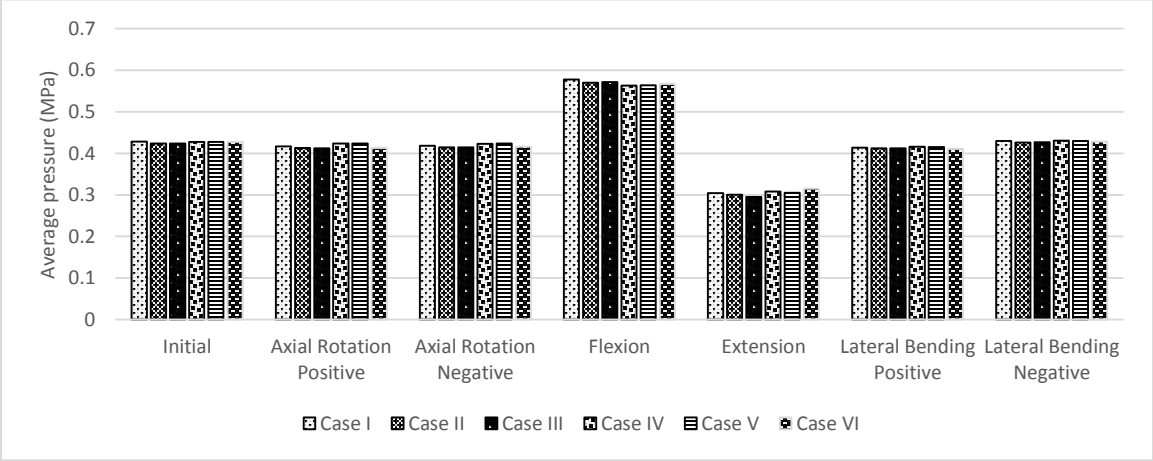

Figure B--4: Average nucleus pulposus pressure in L3-L4

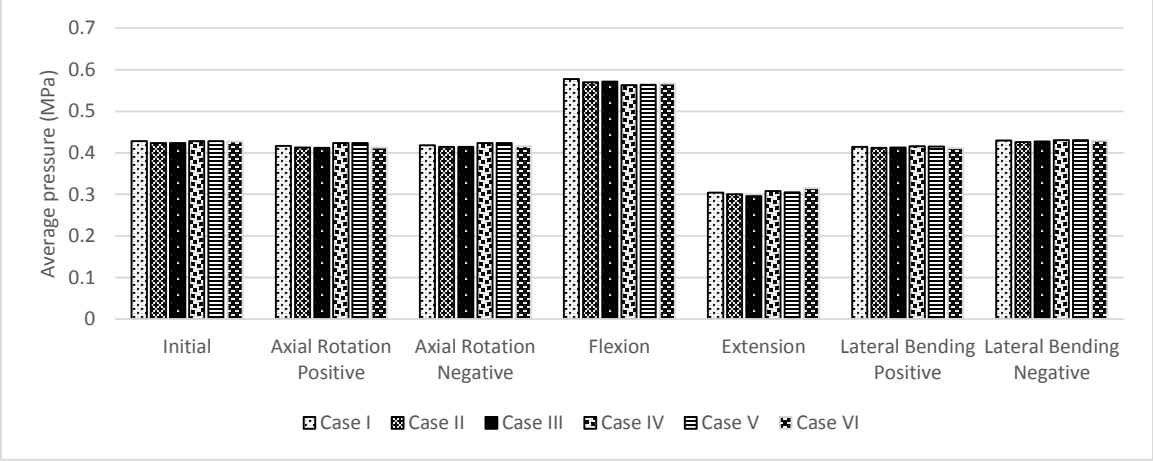

Figure B--5: Average nucleus pulposus pressure in L4-L5

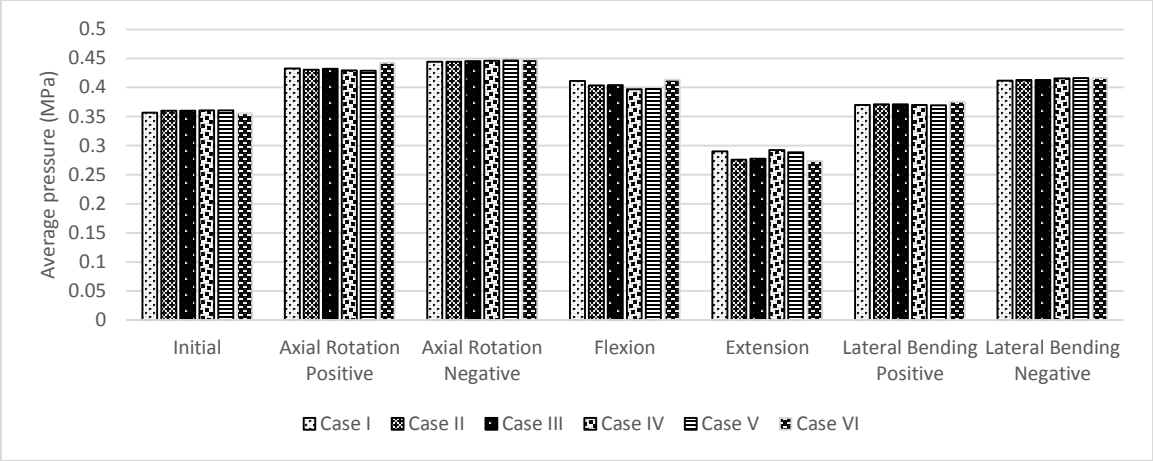

Figure B--6: Average nucleus pulposus pressure in L5-S1

APPENDIX C. BONE STRAIN ENERGY RESULTS

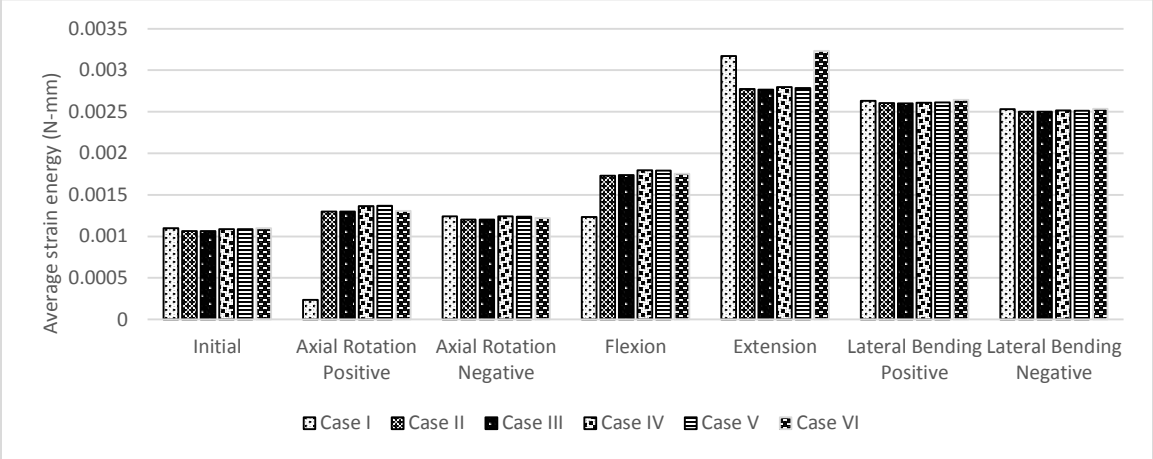

Figure C--1: Average strain energy in L1

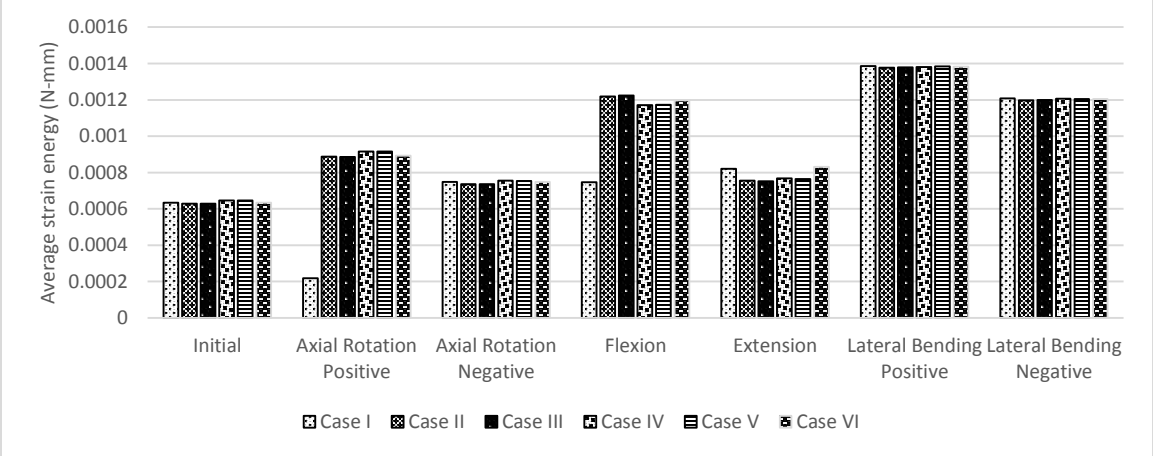

Figure C--2: Average strain energy in L2

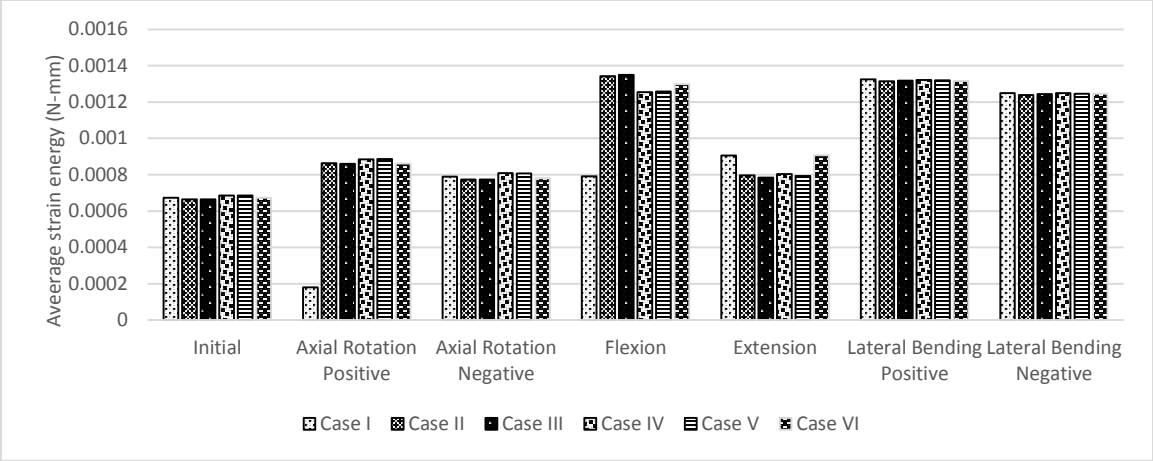

Figure C--3: Average strain energy in L3

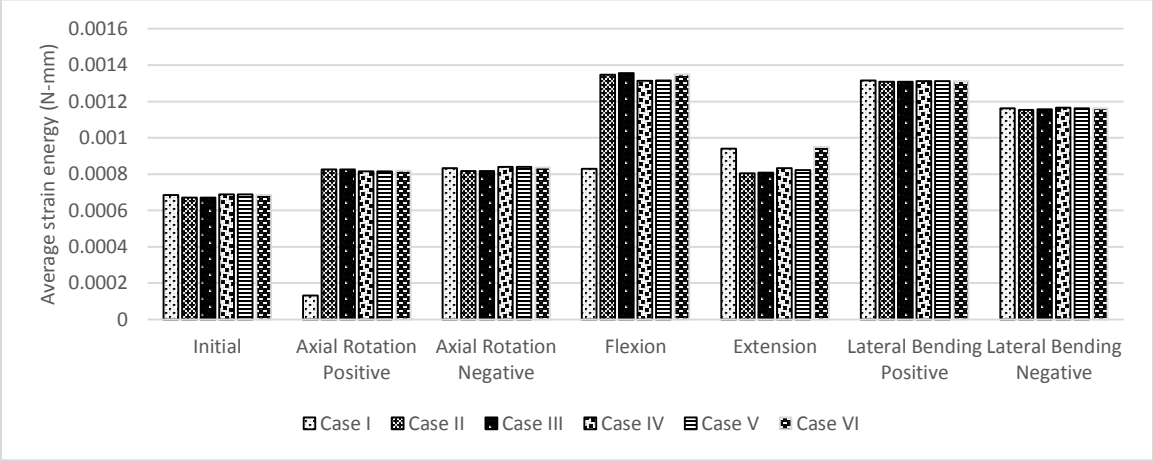

Figure C--4: Average strain energy in L4

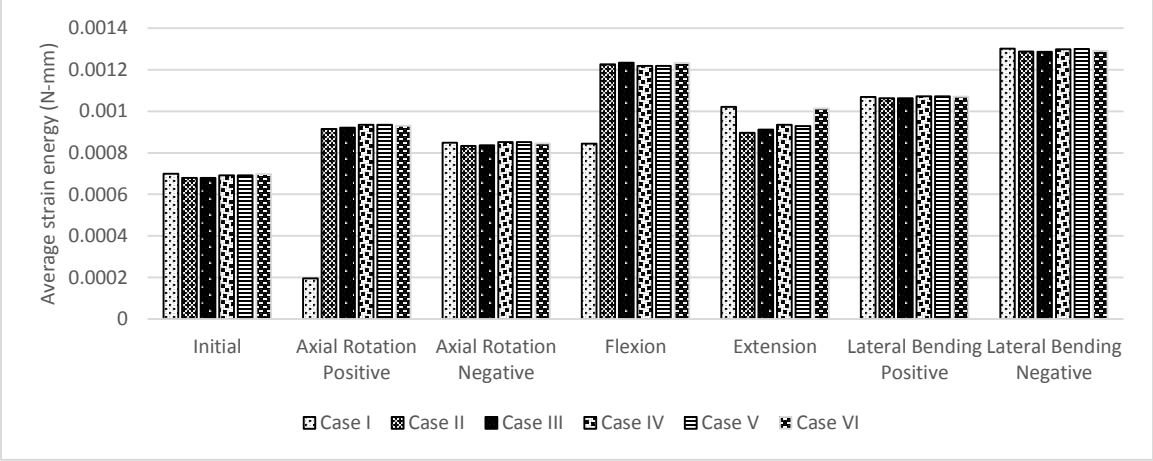

Figure C--5: Average strain energy in L5

APPENDIX D. TORQUE-ROTATON CURVES

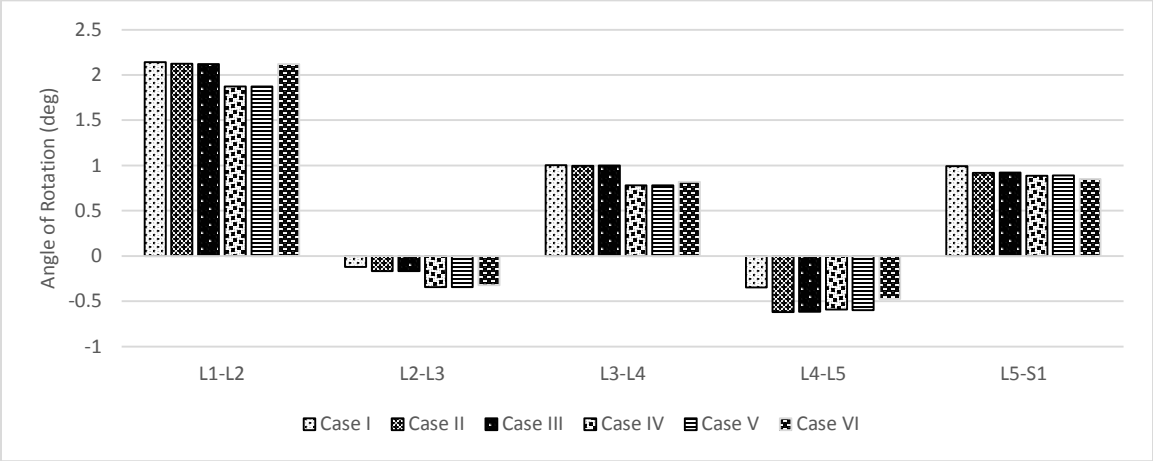

Figure D--1: Angles of rotation during positive axial rotation

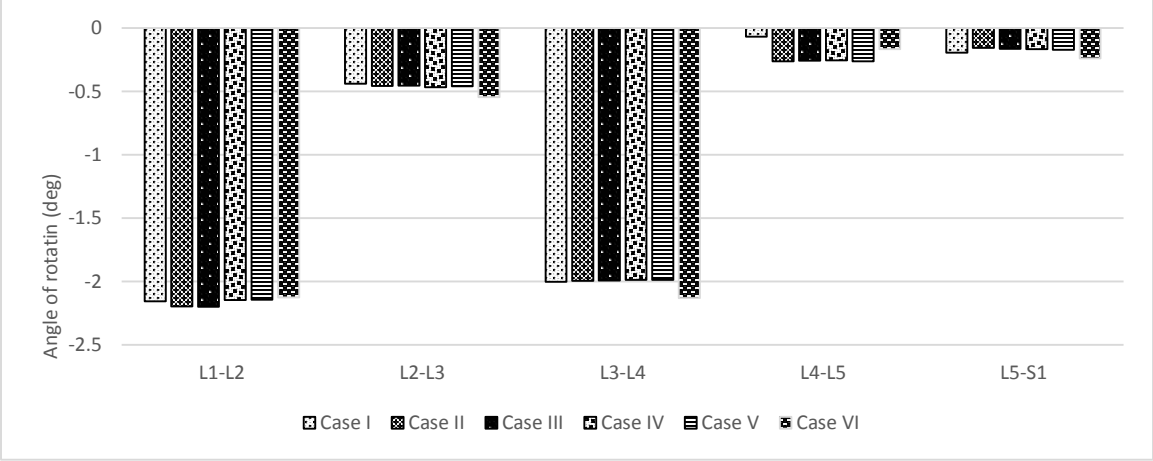

Figure D--2: Angles of rotation during negative axial rotation

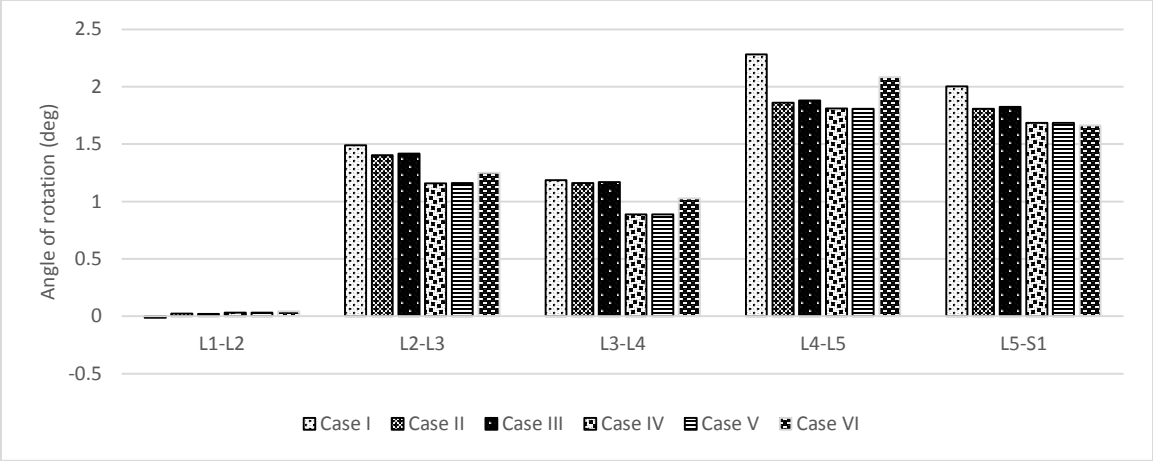

Figure D--3: Angles of rotation during flexion

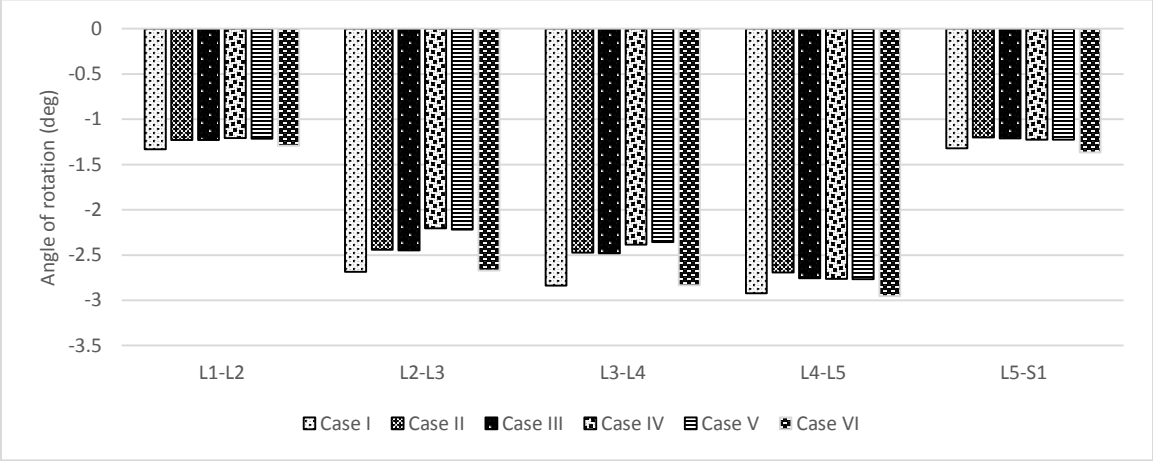

Figure D--4: Angles of rotation during extension

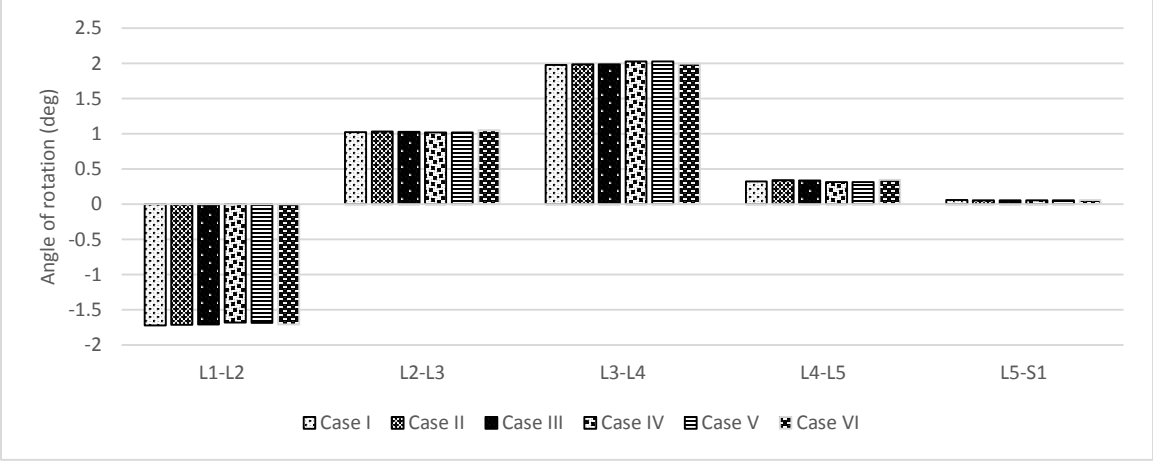

Figure D--5: Angles of rotation during positive lateral bending

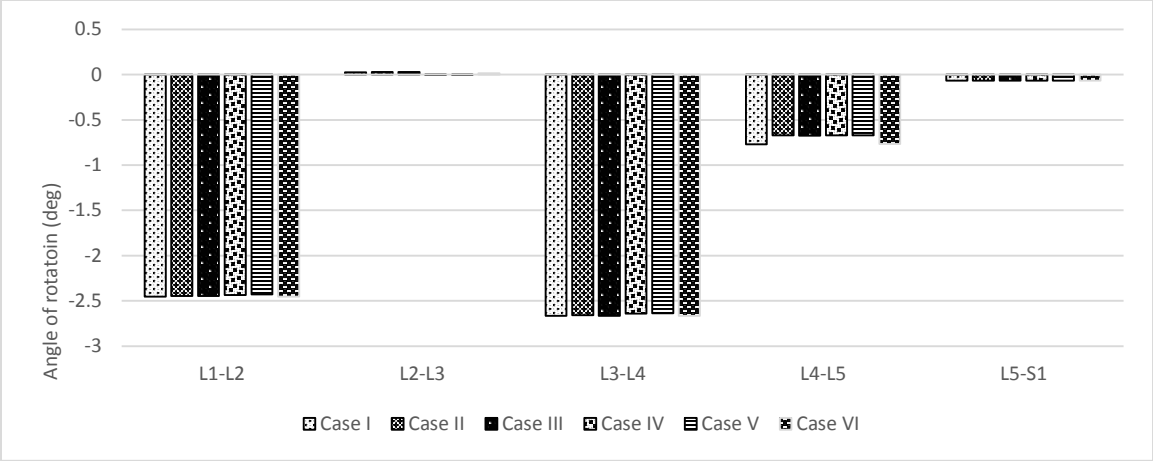

Figure D--6: Angles of rotation during negative axial rotation

APPENDIX F. LOADING FILES

The following are LS-DYNA keyword files that were used in modifying the existing finite element model. For details regarding unmodified components, the readers are referred to the original work by Von Forell et al. [52]

F.1 Updated material model syntax

ALL

```
$
$ DEFINITION OF MATERIAL     26
$
*MAT_SOFT_TISSUE
26,1.0003E-03,0.0951,0.0,0.807,4.077,13.936
100,1.221,0.0,0.0,0.0,0,0
0.0,0.0,0.0,0.0,0.0,0.0,0.0
0.0,0.0,0.0,1
*HOURGLASS
26,0,0.0,0,0.0,0.0
*SECTION_SHELL
26,1,0.0,3.0,0.0,0.0,1
0.9398,0.9398,0.9398,0.9398,0.0
0,90,0
*PART
ALL
26,26,26,0,26,0,0,0
```

SSL

```
$ DEFINITION OF MATERIAL     29
$
*MAT_SOFT_TISSUE
29,1.0003E-03,0.17,0.0,0.6,11.88,19.24
100,1.06,0.0,0.0
0.0,0.0,0.0,0.0,0.0,0.0,0.0
```

```
0.0,0.0,0.0,1
*HOURGLASS
29,0,0.0,0,0.0,0.0
*SECTION_SHELL
29,1,0.0,3.0,0.0,0.0,1
5.0800,5.0800,5.0800,5.0800,0.0
0,90,0
*PART
SSL
29,29,29,0,29,0,0,0
```

ISL

```
$
$ DEFINITION OF MATERIAL     30
$
*MAT_SOFT_TISSUE
30,1.0003E-03,0.27,0.0,0.62,13.27,20.08
100,1.09,0.0,0.0
0.0,0.0,0.0,0.0,0.0,0.0,0.0
0.0,0.0,0.0,1
*HOURGLASS
30,0,0.0,0,0.0,0.0
*SECTION_SHELL
30,1,0.0,3.0,0.0,0.0,1
1.7780,1.7780,1.7780,1.7780,0.0
0,90,0
*PART
ISL
30,30,30,0,30,0,0,0
```

F.2 Localized SSL material properties syntax

```
$ DEFINITION OF MATERIAL     29
$
*MAT_SOFT_TISSUE
29,1.0003E-03,0.15,0.0,0.6,16.37,25.74
100,1.06,0.0,0.0
0.0,0.0,0.0,0.0,0.0,0.0,0.0
0.0,0.0,0.0,1
*HOURGLASS
29,0,0.0,0,0.0,0.0
*SECTION_SHELL
29,1,0.0,3.0,0.0,0.0,1
1.693,1.693,1.693,1.693,-3
0,90,0
```

```
*PART
SSL_VENTRAL
29,29,29,0,29,0,0,0
$ DEFINITION OF MATERIAL     70
$
*MAT_SOFT_TISSUE
70,1.0003E-03,0.16,0.0,0.76,9.66,12.57
100,1.06,0.0,0.0
0.0,0.0,0.0,0.0,0.0,0.0,0.0
0.0,0.0,0.0,1
*HOURGLASS
70,0,0.0,0,0.0,0.0
*SECTION_SHELL
70,1,0.0,3.0,0.0,0.0,1
1.693,1.693,1.693,1.693,0.0
0,90,0
*PART
SSL_MID
70,70,70,0,70,0,0,0
$
$ DEFINITION OF MATERIAL     71
$
*MAT_SOFT_TISSUE
71,1.0003E-03,0.2,0.0,0.54,9.46,14.93
100,1.06,0.0,0.0
0.0,0.0,0.0,0.0,0.0,0.0,0.0
0.0,0.0,0.0,1
*HOURGLASS
71,0,0.0,0,0.0,0.0
*SECTION_SHELL
71,1,0.0,3.0,0.0,0.0,1
1.693,1.693,1.693,1.693,3
0,90,0
*PART
SSL_DORSAL
71,71,71,0,71,0,0,0
*END
```

F.3 In situ strain keyword syntax

Example of initial stress card for one element

```
*INITIAL_STRESS_SHELL
$#L1_ALL
4318,1,3,16,0,0,0,0
0.000E+00,1.704E-01,1.252E-02,5.669E-01,-2.382E-02,-7.084E-02,-1.408E-02,1.098E+00
5.720E-01,1.000E+00,0.000E+00,1.499E+00,1.804E-02,1.094E+00,3.542E-02,-5.036E-03
3.796E-02,1.041E+00,-4.188E-03,-4.783E-03,-3.636E-03,8.807E-01,9.876E+03,1.000E+00
```

```
-7.746E-01,1.438E-01,1.293E-02,5.924E-01,-2.214E-02,-7.615E-02,2.091E-03,1.103E+00
5.952E-01,1.000E+00,0.000E+00,1.499E+00,1.804E-02,1.097E+00,4.843E-02,-4.973E-03
5.500E-02,1.031E+00,-4.265E-03,-4.965E-03,-3.486E-03,8.878E-01,9.876E+03,1.000E+00
7.746E-01,1.977E-01,1.214E-02,5.437E-01,-2.554E-02,-6.576E-02,-3.055E-02,1.093E+00
5.522E-01,1.000E+00,0.000E+00,1.499E+00,1.804E-02,1.091E+00,2.240E-02,-5.097E-03
2.033E-02,1.052E+00,-4.093E-03,-4.595E-03,-3.764E-03,8.738E-01,9.876E+03,1.000E+00
```

F.4 Beam material model syntax

```
*PART
$# title
ALLBeam
$#     pid     secid       mid     eosid      hgid      grav    adpopt      tmid
        70        70        88         0        70         0         0         0
*SECTION_BEAM_TITLE
ALLSection
$#   secid    elform      shrf   qr/irid       cst     scoor       nsm
        70         6  1.000000         2         0     0.000     0.000
$#     vol      iner       cid        ca    offset     rrcon     srcon     trcon
     0.000     0.000         0     2.52     0.000     0.000     0.000     0.000
*MAT_CABLE_DISCRETE_BEAM_TITLE
ALLMAT
$#     mid        ro         e      lcid        f0    tmaxf0     tramp     iread
        88 1.0000E-3 13.936000        0.     0.000     0.000     0.000         0
1
*HOURGLASS_TITLE
ALLHG
$#    hgid       ihq        qm       ibq        q1        q2    qb/vdc        qw
        70         1  0.100000         0  1.500000 6.0000E-2  0.100000  0.100000
*PART
$# title
SSLBeam
$#     pid     secid       mid     eosid      hgid      grav    adpopt      tmid
        71        71        89         0        71         0         0         0
*SECTION_BEAM_TITLE
SSLSection
$#   secid    elform      shrf   qr/irid       cst     scoor       nsm
        71         6  1.000000         2         0     0.000     0.000
$#     vol      iner       cid        ca    offset     rrcon     srcon     trcon
     0.000     0.000         0     3.42     0.000     0.000     0.000     0.000
*MAT_CABLE_DISCRETE_BEAM_TITLE
SSLMAT
$#     mid        ro         e      lcid        f0    tmaxf0     tramp     iread
        89 1.0000E-3 19.240000        0.     0.000     0.000     0.000         0
1
*HOURGLASS_TITLE
SSLHG
$#    hgid       ihq        qm       ibq        q1        q2    qb/vdc        qw
        71         1  0.100000         0  1.500000 6.0000E-2  0.100000  0.100000
*PART
$# title
ISLBeam
$#     pid     secid       mid     eosid      hgid      grav    adpopt      tmid
        72        72        90         0        72         0         0         0
*SECTION_BEAM_TITLE
ISLSection
$#   secid    elform      shrf   qr/irid       cst     scoor       nsm
        72         6  1.000000         2         0     0.000     0.000
$#     vol      iner       cid        ca    offset     rrcon     srcon     trcon
     0.000     0.000         0     1.26     0.000     0.000     0.000     0.000
*MAT_CABLE_DISCRETE_BEAM_TITLE
```

```
ISLMAT
$#     mid        ro         e      lcid        f0    tmaxf0     tramp     iread
        90 1.0000E-3 20.080000         0.     0.000     0.000     0.000         0
1
*HOURGLASS_TITLE
ISLHG
$#    hgid       ihq        qm       ibq        q1        q2    qb/vdc        qw
        72         1  0.100000         0  1.500000 6.0000E-2  0.100000  0.100000
```

F.5 Loading files

Typical follower compression load

```
*KEYWORD
*TITLE
Compression
*CONTROL_TERMINATION
30
*CONTROL_TIMESTEP
,0.8,,,-6.0e-7
*CONTROL_ENERGY
2
*CONTROL_CONTACT
,,2

*CONTROL_SHELL

,1,
*DATABASE_EXTENT_BINARY
,,,1

$
$
*DAMPING_GLOBAL
0,2
*DATABASE_BINARY_D3PLOT
30
*DATABASE_GLSTAT
1
*DATABASE_MATSUM
1
*DATABASE_BNDOUT
1
*DATABASE_RBDOUT
1
*DATABASE_RCFORC
0.002
$*DATABASE_BINARY_INTFORC
```

```
$0.002
$
*INCLUDE
Mats.k
*INCLUDE
Mesh.k
*INCLUDE
Temps.k
*CONSTRAINED_RIGID_BODIES
1,67
*CONSTRAINED_RIGID_BODIES
1,68
*CONSTRAINED_EXTRA_NODES_SET
1,100
$
```

Typical loading after compression

```
*KEYWORD
*CONTROL_TERMINATION
650
*DAMPING_GLOBAL
0,.19
*DATABASE_BINARY_D3PLOT
1
*DATABASE_BINARY_RUNRSF
100000,1,
*CHANGE_CURVE_DEFINITION
1
*DEFINE_CURVE
1
0,0
30,0
590,-6000
1200,-6000
*END
```

F.6 Supercomputer input decks

Typical follower compression input deck

```
#!/bin/bash

#SBATCH --time=80:00:00
#SBATCH --ntasks=12
#SBATCH --nodes=1
#SBATCH --mem-per-cpu=4096M
```

```
#SBATCH --gid=fslg_SpineFEA

export OMP_NUM_THREADS=12
export LSTC_LICENSE=network
export LSTC_LICENSE_SERVER=fsllinuxlic4
export LSTC_LICENSE_SERVER_PORT=13373

/fslhome/mshortin/fsl_groups/fslg_SpineFEA/bin/ls-
dyna_smp_d_r7_0_0_x64_redhat57_ifort101 memory=1000m ncpu=12  i=Load.k
```

Typical load input deck

```
#!/bin/bash

#SBATCH --time=72:00:00
#SBATCH --ntasks=12
#SBATCH --nodes=1
#SBATCH --mem-per-cpu=4096M
#SBATCH --gid=fslg_SpineFEA

export OMP_NUM_THREADS=12
export LSTC_LICENSE=network
export LSTC_LICENSE_SERVER=fsllinuxlic4
export LSTC_LICENSE_SERVER_PORT=13373

/fslhome/mshortin/fsl_groups/fslg_SpineFEA/bin/ls-
dyna_smp_d_r7_0_0_x64_redhat57_ifort101 memory=4000m ncpu=12  i=add.k R=runrsf
```